Efficient Light Harvesting by Using Green Zn-Porphyrin-Sensitized Nanocrystalline TiO_2 Films

Qing Wang,[†] Wayne M. Campbell,[‡] Edia E. Bonfantani,[‡] Kenneth W. Jolley,[‡] David L. Officer,*[,‡] Penny J. Walsh,[§] Keith Gordon,[§] Robin Humphry-Baker,[†] Mohammad K. Nazeeruddin,*[,†] and Michael Grätzel*[,†]

Laboratory for Photonics and Interfaces, Institute of Chemical Sciences and Engineering, Swiss Federal Institute of Technology, CH-1015 Lausanne, Switzerland, Nanomaterials Research Centre and MacDiarmid Institute for Advanced Materials and Nanotechnology, Massey University, Palmerston North, New Zealand, and MacDiarmid Institute for Advanced Materials and Nanotechnology, Chemistry Department, University of Otago, Dunedin, New Zealand

Received: May 31, 2005

A series of novel zinc metalloporphyrins, cyano-3-(2′-(5′,10′,15′,20′-tetraphenylporphyrinato zinc(II))yl)-acrylic acid (**Zn-3**), 3-(*trans*-2′-(5′,10′,15′,20′-tetraphenylporphyrinato zinc(II))yl)-acrylic acid (**Zn-5**), 2-cyano-5-(2′-(5′,10′,15′,20′-tetraphenylporphyrinato zinc(II))yl)-penta-2,4-dienoic acid (**Zn-8**), 4-(*trans*-2′-(2″-(5″,-10″,15″,20″-tetraphenylporphyrinato zinc(II))yl)ethen-1′-yl))-1,2-benzenedicarboxylic acid (**Zn-11**), and 2-cyano-3-[4′-(*trans*-2″-(2‴-(5‴,10‴,15‴,20‴-tetraphenylporphyrinato zinc(II))yl) ethen-1″-yl)-phenyl]-acrylic acid (**Zn-13**) were synthesized and characterized by using various spectroscopic techniques. Density functional theory (DFT) and time-dependent DFT (TDDFT) calculations show that key molecular orbitals (MOs) of porphyrins **Zn-5** and **Zn-3** are stabilized and extended out onto the substituent by π-conjugation, causing enhancement and red shifts of visible transitions and increasing the possibility of electron transfer from the substituent. The porphyrins were investigated for conversion of sunlight into electricity by constructing dye-sensitized TiO_2 solar cells using an I^-/I_3^- electrolyte. The cells yield close to 85% incident photon-to-current efficiencies (IPCEs), and under standard AM 1.5 sunlight, the **Zn-3**-sensitized solar cell demonstrates a short circuit photocurrent density of 13.0 ± 0.5 mA/cm^2, an open-circuit voltage of 610 ± 50 mV, and a fill factor of 0.70 ± 0.03. This corresponds to an overall conversion efficiency of 5.6%, making it the most efficient porphyrin-sensitized solar cell reported to date.

I. Introduction

Photoinduced interfacial charge transfer between a discrete molecular excited state and a continuum of acceptor levels in a solid is an important photochemical surface reaction[1] that influences the performance of dye-sensitized solar cells.[2−4] In contrast to conventional solar cell systems, where the semiconductor assumes both the task of light absorption and charge carrier, in dye-sensitized solar cells light is absorbed by the anchored dye and charge separation takes place at the interface via photoinduced electron injection from the dye into the conduction band of the solid. During the last 10 years, with the development of nanocrystalline films of very high surface area,[5] the photosensitization of wide-band-gap semiconductors such as TiO_2 by adsorbed dyes has become more realistic for solar cell applications.[6−10] In a porous film consisting of nanometer-sized TiO_2 particles, the effective surface area for dye adsorption can be greatly enhanced and efficient light absorption is achieved from dye monolayers.[11]

For a molecular/semiconductor junction light-harvesting system, the first requirement is that the sensitizing dye absorbs light over a wide wavelength range, preferably one that encompasses the visible spectrum. Another essential property is efficient electron transfer from the excited dye to the TiO_2 conduction band; i.e., good electronic coupling between the lowest unoccupied orbital (LUMO) of the dye and the Ti 3d orbitals is required. Effective coupling has typically been accomplished with carboxylate or phosphonate groups, which bind tightly to the TiO_2 surface via a bridging bidentate mode.[12,13] To date, ruthenium polypyridyl complexes have proven to be the most efficient TiO_2 sensitizers, with the N3 dye demonstrating incident photon-to-electron conversion efficiencies (IPCEs) of up to 85% from 400 to 800 nm and an overall photovoltaic cell energy conversion efficiency (η) of 11%.[4,6]

Nature accomplishes enhanced light absorption by stacking chlorophyll-containing thylakoid membranes of the chloroplast to form the grana structures that act as light-harvesting antenna.[14] These absorb the incident light and then channel the excitation energy to reaction centers, where light-induced charge separation takes place.[15] Given their primary role in photosynthesis, the use of porphyrins as light harvesters on semiconductors is particularly attractive. Owing to the delocalized macrocyclic structure and very strong absorption in the 400−450 nm region (Soret band) as well as absorption in the 500−700 nm region (Q-bands), porphyrins have long been studied as promising components of molecular electronic and photonic devices,[16,17] and numerous artificial photonic assemblies based on multi-

* Authors to whom correspondence should be addressed. Phone: 0041-21-693 6124 (M.K.N.). Fax: 0041-21-693 4111 (M.K.N.). E-mail: D.Officer@massey.ac.nz; MdKhaja.Nazeeruddin@epfl.ch; michael.graetzel@epfl.ch.

[†] Swiss Federal Institute of Technology.

[‡] Massey University.

[§] University of Otago

10.1021/jp052877w CCC: $30.25
Published on Web 07/21/2005

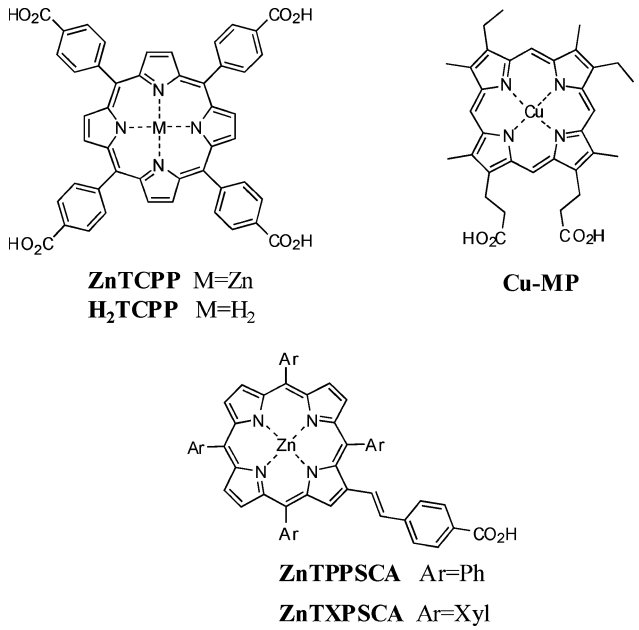

Figure 1. Structures of porphyrin sensitizers.

porphyrin architectures have been designed to mimic photosynthetic solar energy transduction by converting excitation energy to chemical potential in the form of long-lived charge separation.[18−20]

Since the earliest reports of the efficient charge injection into nanocrystalline TiO_2 by covalently bound zinc tetrakis(4-carboxyphenyl)porphyrin (ZnTCPP, Figure 1),[21−23] the photosensitization of TiO_2 electrodes by porphyrins has been extensively studied. It has been demonstrated that, despite the differences in oxidation potentials and photophysics between carboxylated porphyrin sensitizers such as ZnTCPP and its free-base H_2TCPP (Figure 1) and the ruthenium polypyridyl N3 dye, the efficiency of electron injection into the TiO_2 conduction band and the kinetics of electron injection and recombination are indistinguishable for all these sensitizers.[24] In addition, the rate of charge recombination between conduction band electrons and oxidized porphyrins is in the range of several milliseconds, a time that is sufficiently slow to permit the regeneration of the ground state of the porphyrin by the iodide in the electrolyte.[25] Despite these observations, porphyrins have not proven to be as efficient sensitizers as ruthenium polypyridyl dyes.

For photovoltaic cells with H_2TCPP-sensitized TiO_2 electrodes, Cherian and Wamser have reported IPCE values of 25−55% and a η of 3%,[26] although other groups have obtained somewhat lower IPCE and η values for H_2TCPP,[25,27−29] ZnTCPP,[30] and similar porphyrins.[25,29−31] These differences have been ascribed to aggregation, the effect of coadsorbates, and poor electronic interaction between the carboxylate linker and the porphyrin core. This latter issue had been addressed by Grätzel and co-workers who investigated the sensitization of TiO_2 with a variety of chlorophyll derivatives and related mesoporphyrins.[32] They obtained IPCE values of over 80% and a η value of 2.6% for a TiO_2 electrode sensitized with copper mesoporphyrin (CuMP, Figure 1), leading to the conclusion that conjugation of the carboxyl group with the π-electron system of the chromophore is not essential for efficient electron transfer. Recently, however, Campbell et al. demonstrated a 40% increase in cell efficiency ($\eta = 4.2\%$) for a tetraphenylporphyrin with a β-substituted styrylcarboxylic acid (ZnTPPSCA, Figure 1), the single acid linker being in full conjugation with the porphyrin π system; removal of the conjugation resulted in a halving of the η value.[12,30] Cell efficiency was also found to be susceptible to porphyrin metalation, type of acid binder, acid position, binding solvent, and the electrolyte used.[30] Replacement of the porphyrin phenyl substituents with xylyl groups, ZnTXPSCA (Figure 1), further improved cell efficiency ($\eta = 4.8\%$).[12] It is apparent from these studies that the strength of binding of the dye to the semiconductor has a significant influence on the cell efficiency, and this presents the opportunity to explore both the nature of the linker and the type of carboxylic acid in this type of conjugatively substituted porphyrin.

The modification of *meso*-tetraphenylporphyrins by substitution at the β-position with functional groups with extended π systems, leads to the enhancement of the red-absorbing Q-bands.[33] This is caused by the splitting of the four frontier molecular orbitals (FMOs) of Gouterman's four-orbital model.[34] Computational chemistry offers an opportunity to gain insight into the electronic processes, which occur in the FMOs of porphyrins. Local and nonhybrid methods including LSDA,[35] BP86,[36] and PW91[37] significantly underestimate the oscillator strengths (*f*) of the B-bands and give deviations in the energies of the transitions of 0.5−1.1 eV. However, density functional theory (DFT) methods such as B3LYP[38] have been found to rival the multireference perturbation theory (PT2) and couple cluster (SAC-CI, CC) methods for these systems.[39] A number of comparisons between calculated ground-state absorption spectra using various functionals have been made.[40−42] Calculations using hybrid functionals such as B3LYP are more accurate over a wider spectral range.

In this paper, we report the electrochemical, photophysical, and photoelectrochemical properties of a series of novel green Zn porphyrins as well as density functional theory (DFT) and time-dependent DFT (TDDFT) calculations on zinc tetraphenylporphyrin (ZnTPP), **Zn-3**, and **Zn-5**. It will be shown that the nature of the carboxylic acid linker to the porphyrin has a significant influence on the light-harvesting and photovoltaic properties of the device and that a cell that utilizing the dye **Zn-3** exhibits an efficiency of 5.6%, the best value achieved so far for a porphyrin dye.

II. Experimental Section

A. Materials and General Synthetic Procedures. Analytical reagent grade solvents and reagents were used for synthesis, and distilled laboratory grade solvents were used for chromatography. Reverse osmosis or Milli-Q water was used for synthetic and purification purposes. Dry toluene and tetrahydrofuran (THF) were prepared by passing argon-degassed solvent through activated alumina columns. N_2 (oxygen-free) was passed through a KOH drying column to remove moisture. The intermediate compounds TPP−CHO **1** (Scheme 1) and TPPps **10** (Scheme 2) were prepared according to Bonfantini et al.[43] TPP═PhCHO **12** (Scheme 2) was synthesized according to Officer et al.[44]

Column chromatography employed silica gel (0.032−0.063 mm, Merck Kieselgel 60) or the equivalent. Thin-layer chromatography (TLC) was performed using precoated silica gel plates (Merck Kieselgel $60F_{254}$). Either gravity or flash chromatography was used for compound purification. Where a dual solvent system was used, gradient elution was employed, and the major band was collected. All fractions or solutions containing a single spot by TLC with the same R_f were combined and filtered, and the solvent was removed in vacuo (rotary evaporation followed by high vacuum). All solid precipitates were separated by filtration or centrifugation, rinsing with the precipitating solvent, then dried under high vacuum

SCHEME 1: Synthesis of β-Ethenyl Carboxylic Acids

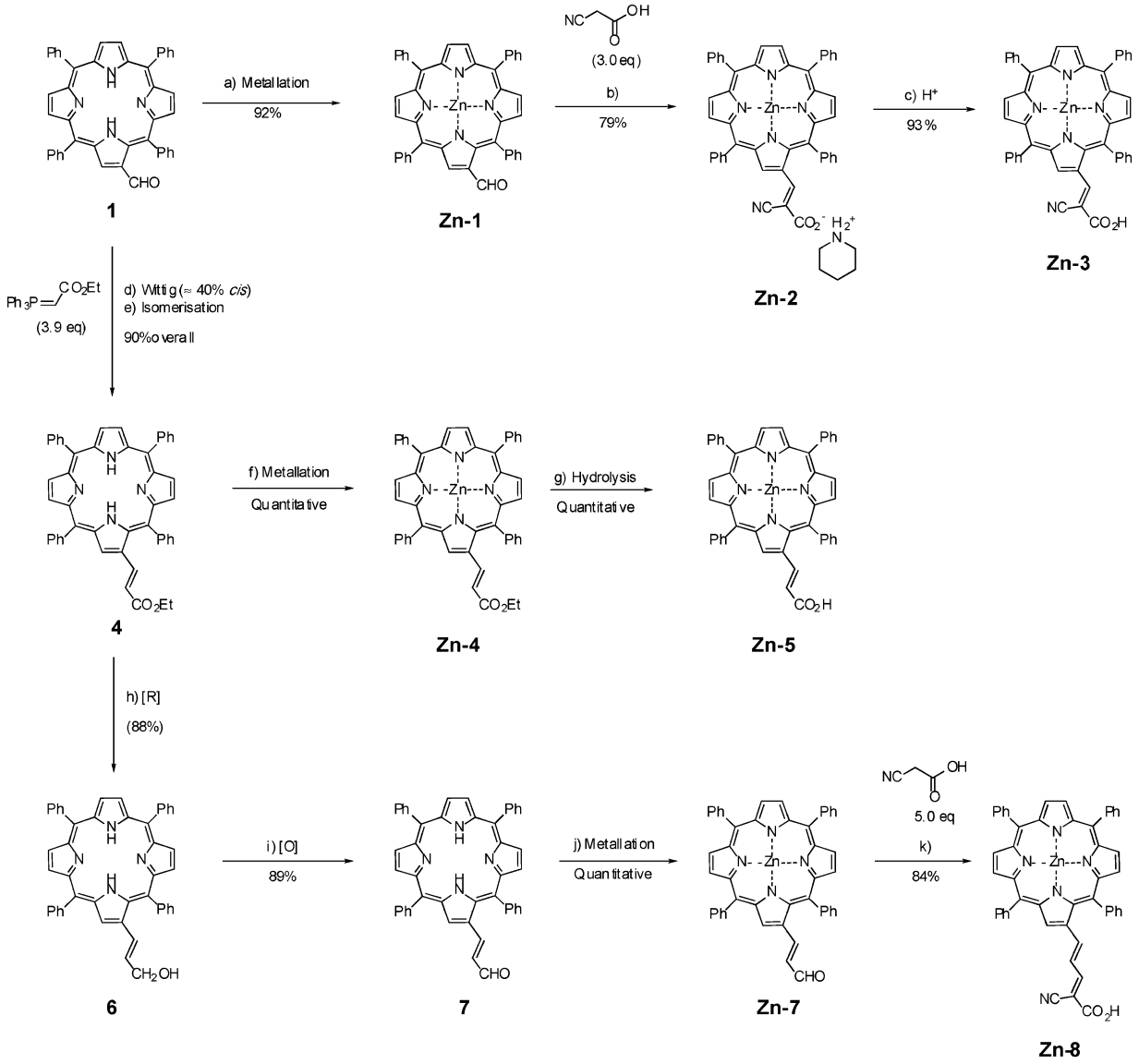

[a] $Zn(OAc)_2 \cdot 2H_2O$, MeOH/$CHCl_3$, room temperature (20 min). [b]Piperidine (22 equiv), acetonitrile, reflux (2.5 h), N_2. [c]H_3PO_4 (2 M, pH $\approx$ 2.0). [d]Toluene, reflux (23.5 h), N_2. [e](i) I_2 (1.0 equiv), $CHCl_3$, room temperature (14 h); (ii) saturated $Na_2S_2O_3$ (excess). [f]$Zn(OAc)_2 \cdot 2H_2O$ (1.2 equiv), $CHCl_3$/MeOH, room temperature (30 min). [g](i) NaOH (20 equiv), THF/H_2O/EtOH (5:1:5), reflux (40 min); (ii) H_3PO_4 (2 M, pH $\approx$ 2.5). [h](i) DIBAL−H (3.0 equiv), toluene, 0 °C → room temperature → 0 °C, argon; (ii) MeOH. [i]MnO_2 (excess), CH_2Cl_2, room temperature. [j]$Zn(OAc)_2 \cdot 2H_2O$ (1.2 equiv), MeOH/$CHCl_3$, room temperature (10 min). [k](i) Piperidine (24 equiv), MeOH, reflux (50 min), N_2; (ii) H^+.

overnight. All porphyrin reactions were carried out under a nitrogen or argon atmosphere using dry degassed solvents, and the apparatus was shielded from ambient light.

B. Analytical Measurements. UV−vis absorption spectra were measured on a Cary 5 spectrophotometer, and fluorescence spectra were recorded on a Spex Fluorolog 112 spectrofluorimeter. Samples were contained in 1-cm path-length quartz cells. Emission lifetimes were measured by exciting with a pulse from an active mode-locked Nd:YAG laser, using the frequency-doubled line at 532 nm. The emission decay was followed on a Tektronix DSA 640 digitizing signal analyzer, using a Hamamatsu R928 photomultiplier to convert the light signal to a voltage waveform.

Fast-atom bombardment (FAB) mass spectra were recorded on a Varian VG70-SE double-focusing magnetic sector mass spectrometer. Samples were supported in a *m*-nitrobenzyl alcohol matrix. The data were put through a MASSPEC II data system to give ±5 ppm error formulations on molecular ions. Major fragmentations are given as percentages relative to the base peak intensity.

^{1}H NMR spectra were obtained at 400.132 MHz using a Bruker 400 Avance NMR spectrometer running X-WIN NMR software. The chemical shifts are relative to tetramethylsilane (TMS).

Voltammetric measurements were performed on a PC-controlled AutoLab PSTAT10 electrochemical workstation (Eco Chemie). Cyclic voltammetry experiments were performed on 1 mM Zn porphyrin solutions in dimethylformamide (DMF) at a scan rate of 0.1 V/s using 0.1 M tetra-*n*-butylammonium hexafluorophosphate ($TBAPF_6$) as the supporting electrolyte and a 2 mm platinum disk as the working electrode. After a cyclic voltammogram (CV) had been recorded, ferrocene was added, and a second voltammogram was measured. For measurements made on Zn porphyrins adsorbed onto TiO_2 films, the electrolyte was 0.2 M $TBAPF_6$ in acetonitrile. Platinum foil and a silver

SCHEME 2: Synthesis of β-Styryl Carboxylic Acids

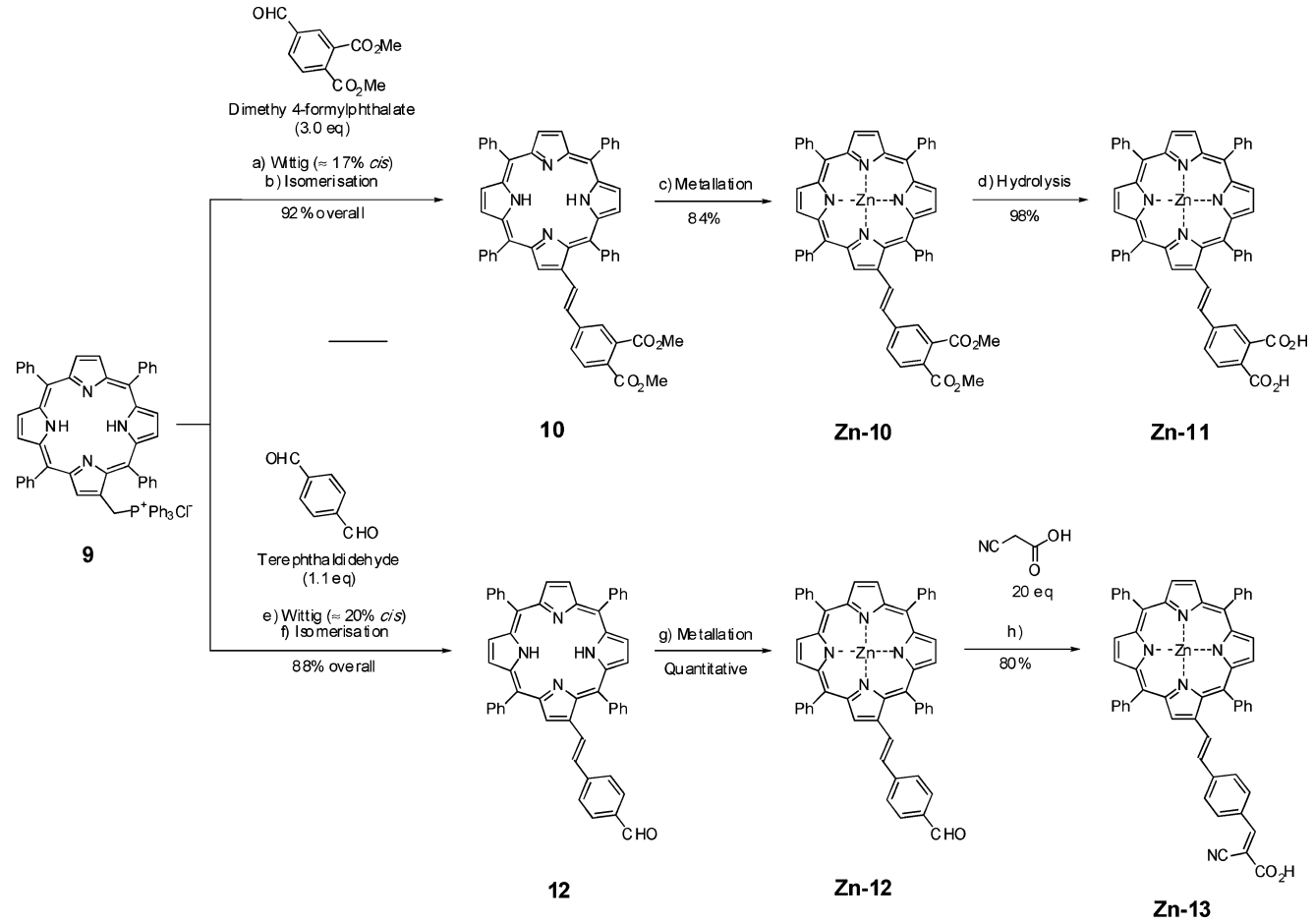

[a] DBU (3.0 equiv), $CHCl_3$, reflux (15 min), N_2. [b](i) I_2 (2.4 equiv), CH_2Cl_2, room temperature (3 h); (ii) saturated $Na_2S_2O_3$ (excess). [c]$Zn(OAc)_2 \cdot 2H_2O$ (1.2 equiv), $CHCl_3$/MeOH, room temperature (15 min). [d](i) NaOH (20 equiv per CO_2Me), THF/H_2O/MeOH (1:0.2:1), reflux (2 h), N_2; (ii) H_3PO_4 (2 M, pH ≈ 2.0). [e]DBU (5.5 equiv), CH_2Cl_2, room temperature (1 min). [f](i) I_2 (0.7 equiv), CH_2Cl_2, room temperature (16 h); (ii) saturated $Na_2S_2O_3$ (excess). [g]$Zn(OAc)_2 \cdot 2H_2O$ (1.2 equiv), MeOH/$CHCl_3$, room temperature (20 min). [h](i) Piperidine (55 equiv), MeOH, reflux (15 h), argon; (ii) H^+.

disk were employed as the counter and quasi-reference electrode, respectively.

The Fourier transform IR (FTIR) spectra for all the samples were measured using a FTS Digilab 7000 FTIR spectrometer. The attenuated total reflectance (ATR) data reported here was taken with the Golden Gate diamond anvil ATR accessory (Graseby-Specac), using typically 64 scans at a resolution of 2 cm^{-1}. All samples were placed in contact with the diamond window using the same mechanical force. The dye-coated TiO_2 films were rinsed in acetonitrile and dried at 150 °C before measuring the spectra. The FTIR spectra of anchored dyes were obtained by subtracting the IR spectrum of the blank TiO_2 films from the IR spectrum of the dye-coated TiO_2 films of the same thickness.

C. Preparation of Dye-Sensitized Nanocrystalline TiO_2 Electrodes. A paste consisting of 20-nm-sized TiO_2 colloid and ethyl cellulose in terpineol was first screen-printed on a fluorine-doped SnO_2 conducting glass (TEC15, 15 Ω/cm) to form a transparent layer. Subsequently, a second scattering layer made up of a paste containing 400 nm anatase TiO_2 particles (CCIC, Japan) was further coated on it to form a light-scattering layer. Last, the screen-printed double-layer film was heated to 500 °C in an oxygen atmosphere and calcinated for 10 min. The final film thickness was determined by using an Alpha-step 200 surface profilometer (Tencor Instruments). A porosity of 0.63 for the transparent layer was measured with a Gemini 2327 nitrogen adsorption apparatus (Micromeretics Instrument Co.). The TiO_2 plates (electrodes) were dipped into a 2×10^{-4} M dye solution in THF and left for 2 h. Finally, the dye-coated electrodes were rinsed with acetonitrile.

D. Dye-Sensitized Solar Cell Fabrication. A sandwich cell was prepared using the dye-sensitized electrode as the working electrode and a platinum-coated conducting glass electrode as the counter electrode. The latter was prepared by chemical deposition of platinum from 0.05 M hexachloroplatinic acid. The two electrodes were placed on top of each other using a thin transparent film of Surlyn polymer (DuPont) as a spacer to form the electrolyte space. The empty cell was tightly held, and the edges were heated to 130 °C to seal the two electrodes together. A thin layer of electrolyte (0.6 M BMII, 0.05 M I_2, 0.1 M LiI, 0.5 M *tert*-butyl pyridine in 1:1 acetonitrile/valeronitrile) was introduced into the interelectrode space from the counter electrode side through a predrilled hole. The hole was sealed with a microscope cover slide and Surlyn to avoid leakage of the electrolyte solution.

E. Photoelectrochemical Measurements. The photovoltaic performances of the Zn-porphyrin-sensitized nanocrystalline TiO_2 cells were determined using two complementary techniques. The spectral response was determined by measuring the wavelength dependence of the incident photon-to-current conversion efficiency (IPCE) using light from a 300-W xenon lamp (ILC Technology) that was focused onto the cell through a

Gemini-180 double monochromator (Jobin Yvon Ltd., U. K.). The monochromator was incremented through the visible spectrum to generate the IPCE(λ) curve as defined below

$$\mathrm{IPCE}(\lambda) = 12\,400(J_{sc}/\lambda\Phi) \quad (1)$$

where λ is the wavelength (nm), J_{sc} is the photocurrent under short circuit conditions (mA/cm^2), and Φ is the incident radiative flux (mW/cm^2). The whole experiment was run automatically using Wavemetrics Igor Pro software. For $I-V$ measurements, a 450-W xenon light source (Osram XBO 450) was used as the irradiation source. The spectral output of the lamp matched the AM 1.5 solar spectrum in the region of 350−750 nm (mismatch <2%). Incident light intensities were adjusted with neutral wire mesh attenuators. The current−voltage characteristics were determined by applying an external potential bias to the cell and measuring the photocurrent using a Keithley model 2400 digital source meter. The overall conversion efficiency η of the photovoltaic cell is calculated from the integral photocurrent density (J_{sc}), the open-circuit photovoltage (V_{oc}), the fill factor of the cell (ff), and the intensity of the incident light (I_{Ph})

$$\eta = J_{sc}V_{oc}\mathrm{ff}/I_{Ph} \quad (2)$$

F. Computational Methods. The Gaussian 03W package[45] was used to perform calculations for ZnTPP, **Zn-3**, and **Zn-5**. Molecular orbitals were visualized using Gaussview. The geometry optimizations, vibrational frequencies, and time-dependent calculations were performed using DFT (B3LYP/3-21G*). The optimized structure was used to calculate vibrational frequencies. Importantly, none of the frequency calculations generated negative frequencies; this is consistent with an energy minimum for the optimized geometry.

G. Synthesis. *1. 2-Formyl-5,10,15,20-tetraphenylporphyrinato Zinc(II) (**Zn-1**).* A solution of $Zn(OAc)_2{\cdot}2H_2O$ (123 mg, 560 μmol, 1.2 equiv) in MeOH (3.0 mL) was added to a solution of **1**[43] (300 mg, 467 μmol) in $CHCl_3$ (20 mL) with stirring at room temperature. After 20 min, TLC analysis indicated that the reaction was complete with the appearance of a new more polar green band (R_f = 0.10, silica, 2:1 (CH_2Cl_2/hexane). Precipitation using MeOH gave the crude product. Recrystallization from CH_2Cl_2/MeOH gave **Zn-1** (304.7 mg, 92%) as a purple microcrystalline solid. ^{1}H NMR (400 MHz, $CDCl_3$, TMS, δ): 7.71−7.83 (m, 12H, $H_{m,p\text{-Ph}}$), 8.15−8.23 (m, 8H, $H_{o\text{-Ph}}$), 8.88−8.94 (m, 6H, $H_{\beta\text{-pyrrolic}}$), 9.224 (s, 1H, $H_{3''(\beta\text{-pyrrolic})}$), 9.515 (s, CHO). UV−vis (CH_2Cl_2) λ_{max} (nm) (ϵ (10^3 M^{-1} cm^{-1})): 432 (342), 526 (4.08), 560 (15.6), 602 (11.3), 681 (8.39). Fast-atom bombardment low-resolution mass spectroscopy (FAB-LRMS) *m*/*z* (%, assignment): cluster at 704−710, 704 (100, M$^+$). High-resolution mass spectroscopy (HRMS) for M$^+$ ($C_{45}H_{28}N_4OZn$): calcd, 704.1555; found, 704.1542.

*2. 2-Cyano-3-(2′-(5′,10′,15′,20′-tetraphenylporphyrinato Zinc(II))yl)acrylic Acid Piperidine Salt (**Zn-2**).* A solution of **Zn-1** (250 mg, 354 μmol), cyanoacetic acid (90 mg, 1.06 mmol, 3.0 equiv), and piperidine (654 μL, 7.68 mmol, 22 equiv) in acetonitrile (50 mL) was heated at reflux temperature for 1 h. After being cooled to room temperature, the resulting green precipitate was collected by filtration (#4 glass sinter) and rinsed with acetonitrile (2.0 mL). Recrystallization from $CHCl_3$/5% MeOH/acetonitrile gave **Zn-2** (240.2 mg, 79%) as a purple solid. ^{1}H NMR (400 MHz, deuterated dimethylsufoxide (DMSO-d_6), TMS, δ): 1.510 (br s, 6H, $CH_{2,\text{piperidine}}$), 2.716 (br s, 4H, $CH_{2,\text{piperidine}}$), 7.67−7.82 (m, 13H, $12H_{m,p\text{-Ph}} + 1H_3$), 8.01−8.04 (m, 2H, $H_{o\text{-Ph}}$), 8.16−8.21 (m, 6H, $H_{o\text{-Ph}}$), 8.635 and 8.717 (ABq, 2H, ^3J = 4.7, 4.7 Hz, $H_{\beta\text{-pyrrolic}}$), 8.749 (s, 2H, $H_{\beta\text{-pyrrolic}}$), 8.769 and 8.793 (ABq, 2H, ^3J = 4.7, 4.7 Hz, $H_{\beta\text{-pyrrolic}}$), 9.298 (d, 1H, ^4J = 1.1 Hz, $H_{3'(\beta\text{-pyrrolic})}$). Assignments aided by correlation spectroscopy (COSY) spectra. UV−vis (THF) λ_{max} (nm) (ϵ (10^3 M^{-1} cm^{-1})): sh 408 (41.7), 454 (150), 571 (12.6), 620 (11.5). FAB-LRMS *m*/*z* (%, assignment): 86 (100, piperidine$^+$), cluster at 771−778, 771 (25, M$^+$).

*3. 2-Cyano-3-(2′-(5′,10′,15′,20′-tetraphenylporphyrinato Zinc(II))yl)acrylic Acid (**Zn-3**).* **Zn-2** (140 mg, 163 μmol) was dissolved in DMSO-d_6 (1.5 mL). H_2O (150 mL) and $CHCl_3$ (50 mL) were added, and the mixture was transferred to a separating funnel. Next, 2 M H_3PO_4 (2.0 mL) was added, and the mixture was shaken vigorously (pH ≈ 2.0). The organic layer was washed with H_2O (150 mL) containing 2 M H_3PO_4 (1.0 mL) and then carefully separated. The $CHCl_3$ was removed by azeotrope distillation using acetonitrile in vacuo. Precipitation from the resulting acetonitrile solution (∼50 mL) using H_2O gave **Zn-3** (117.7 mg, 93%) as a green powder. ^{1}H NMR (400 MHz, DMSO-d_6, TMS, δ): 7.74−7.85 (m, 12H, $H_{m,p\text{-Ph}}$), 8.07−8.11 (m, 3H, $2H_{o\text{-Ph}} + 1H_3$), 8.15−8.21 (m, 6H, $H_{o\text{-Ph}}$), 8.759 and 8.800 (ABq, 2H, ^3J = 4.7, 4.7 Hz, $H_{\beta\text{-pyrrolic}}$), 8.740 and 8.748 (ABq, 2H, ^3J = 4.7, 4.7 Hz, $H_{\beta\text{-pyrrolic}}$), 8.881 and 8.900 (ABq, 2H, ^3J = 4.7, 4.7 Hz, $H_{\beta\text{-pyrrolic}}$), 9.492 (d, 1H, ^4J = 1.0 Hz, $H_{3'(\beta\text{-pyrrolic})}$), 13.470 (br s, 1H, CO_2H). Assignments aided by COSY spectra. UV−vis (THF) λ_{max} (nm) (ϵ (10^3 M^{-1} cm^{-1})): 407 (42.5), sh 429 (92.4), 455 (153), 571 (12.7), 620 (11.9). FAB-LRMS *m*/*z* (%, assignment): cluster at 771−778, 771 (100, M$^+$). HRMS for M$^+$ ($C_{48}H_{29}N_5O_2Zn$): calcd, 771.1613; found, 771.1637.

*4. 3-trans-(5′,10′,15′,20′-Tetraphenylporphyrin-2′-yl)acrylic Acid Ethyl Ester (**4**).* a. Wittig Reaction. A solution of **1** (550 mg, 0.856 mmol) and ethyl (triphenylphosphoranylidene)acetate (1.18 g, 3.38 mmol, 3.9 equiv) in dry toluene (60 mL) was heated at reflux temperature under N_2. After 23.5 h, TLC analysis (silica, toluene) indicated that all of starting material **1** had been consumed. After being cooled to room temperature, the solvent was removed in vacuo. The residue was purified by column chromatography (silica, 45 mm_{dia}, 100 mm, CH_2Cl_2/hexane (2:1)), collecting the major purple fraction to give a cis/trans isomeric mixture of **4** (633 mg, ∼40% cis by ^{1}H NMR, 103%) as a purple solid. ^{1}H NMR (270 MHz, $CDCl_3$, TMS, selected data only, δ): −2.725 (s, NH_{cis}), −2.618 (s, NH_{trans}), 0.833 (t, ^3J = 7.3 Hz, $CH_2-CH_{3\text{-}cis}$), 3.961 (q, ^3J = 7.3 Hz, $CH_2-CH_{3\text{-}cis}$), 5.628 (d, ^3J = 11.9 Hz, $H_{cis\text{-ethenyl}}$), 6.884 (dd, ^3J = 12.4 Hz, ^4J = 1.2 Hz, $H_{cis\text{-ethenyl}}$).

b. Isomerization. The isomeric mixture was dissolved in $CHCl_3$ (40 mL) and I_2 (255 mg, 0.856 mmol, 1.0 equiv) was added. After the solution was stirred at room temperature for 14 h in darkness, excess saturated $Na_2S_2O_3$ (∼20 mL) was added, and stirring continued for 30 min. The organic layer was separated and dried ($MgSO_4$), and the product was precipitated with methanol to give *trans*-**4** (549 mg, 90%) as a dark brown powder. ^{1}H NMR (400 MHz, $CDCl_3$, TMS, δ): −2.619 (s, 2H, NH), 1.360 (t, 3H, ^3J = 7.3 Hz, OCH_2-CH_3), 4.230 (q, 2H, ^3J = 7.1 Hz, OCH_2-CH_3), 6.574 (d, 1H, ^3J = 15.6 Hz, H_2), 7.416 (dd, 1H, ^3J = 15.6 Hz, ^4J = 0.7 Hz, H_3), 7.71−7.86 (m, 12H, $H_{m,p\text{-Ph}}$), 8.11−8.21 (m, 8H, $H_{o\text{-Ph}}$), 8.77−8.84 (m, 6H, $H_{\beta\text{-pyrrolic}}$), 8.975 (s, 1H, $H_{3'(\beta\text{-pyrrolic})}$). UV−vis ($CH_2Cl_2$) λ_{max} (nm) (ϵ (10^3 M^{-1} cm^{-1})): 429 (256), 523 (17.8), 563 (7.44), 601 (6.03), 659 (4.09). FAB-LRMS *m*/*z* (%, assignment): cluster at 712−716, 713 (100, MH$^+$). HRMS for MH$^+$ ($C_{49}H_{37}N_4O_2$): calcd, 713.2917; found, 713.2908.

*5. 3-(trans-2′-(5′,10′,15′,20′-Tetraphenylporphyrinato Zinc(II))yl)acrylic Acid Ethyl Ester (**Zn-4**).* A solution of $Zn(OAc)_2{\cdot}2H_2O$ (73.9 mg, 337 μmol, 1.2 equiv) in MeOH (2.0 mL) was

added to a solution of *trans*-**4** (200 mg, 281 μmol) in $CHCl_3$ (20 mL) with stirring at room temperature under a N_2 atmosphere. After 30 min, TLC analysis (silica, toluene) indicated that all of **4** had been consumed with the appearance of a single new spot at a lower R_f value. The solvent was removed in vacuo, and the residue was purified by column chromatography (silica, 37 mm_{dia} × 60 mm, CH_2Cl_2/hexane (2:1)), collecting the major red-green band to give **Zn-4** (217 mg, 100%) as a purple powder. ^{1}H NMR (400 MHz, $CDCl_3$, TMS, δ): 1.326 (t, 3H, ^3J = 7.1 Hz, OCH_2-CH_3), 4.133 (q, 2H, ^3J = 7.2 Hz, OCH_2-CH_3), 6.449 (d, 1H, ^3J = 15.6 Hz, H_2), 7.391 (dd, 1H, ^3J = 15.6 Hz, ^4J = 0.9 Hz, H_3), 7.69−7.81 (m, 12H, $H_{m,p\text{-Ph}}$), 8.08−8.10 (m, 2H, $H_{o\text{-Ph}}$), 8.18−8.20 (m, 6H, $H_{o\text{-Ph}}$), 8.838 and 8.884 (ABq, 2H, ^3J = 4.7, 4.7 Hz, $H_{\beta\text{-pyrrolic}}$), 8.906 and 8.918 (ABq, 2H, ^3J = 4.7, 4.7 Hz, $H_{\beta\text{-pyrrolic}}$), 8.907 (s, 2H, $H_{\beta\text{-pyrrolic}}$), 9.083 (d, 1H, ^4J = 0.9 Hz, $H_{3'(\beta\text{-pyrrolic})}$). Assignments aided by COSY spectra. UV−vis (CH_2Cl_2) λ_{max} (nm) (ϵ (10^3 M^{-1} cm^{-1})) 432 (330), 556 (21.8), 596 (8.81). FAB-LRMS *m*/*z* (%, assignment): cluster at 774−780, 774 (100, M^+). HRMS for M^+ ($C_{49}H_{34}N_4O_2Zn$): calcd, 774.1973; found, 774.2001.

*6. 3-(trans-2′-(5′,10′,15′,20′-Tetraphenylporphyrinato Zinc-(II))yl)acrylic Acid (**Zn-5**).* A solution of NaOH (156 mg, 20 equiv, 3.9 mmol) in H_2O (3.0 mL) was added to a refluxing solution of **Zn-4** (150 mg, 193 μmol) in THF (15 mL) and ethanol (15 mL) under a N_2 atmosphere. After 90 min, TLC analysis indicated that all of **Zn-4** had been consumed. After the solution was cooled to room temperature, CH_2Cl_2 (200 mL), H_2O (800 mL), Et_2O (600 mL), and aqueous 2 M H_3PO_4 (7.0 mL) was added, and the solution was transferred to a separating funnel and shaken vigorously (pH ≈ 2.5). The organic layer was rinsed with H_2O (200 mL, containing 1.0 mL of aqueous 2 M H_3PO_4), separated, and dried ($MgSO_4$). The solvent was removed in vacuo, and the residue was dissolved in a mixture of warm acetone (∼30 mL) and THF (enough to dissolve all the solid), then filtered (#4 glass sinter). The product was precipitated from solution with H_2O (∼20 mL, containing 4 drops acetic acid) and rinsed with acetone/H_2O (1:1) to give **Zn-5** (146 mg, 100%) as a purple powder. ^{1}H NMR (400 MHz, DMSO-d_6, TMS, δ): 6.424 (d, 1H, ^3J = 15.5 Hz, H_2), 7.327 (d, 1H, ^3J = 15.5 Hz, H_3). 7.73−7.85 (m, 12H, $H_{m,p\text{-Ph}}$), 8.06−8.08 (m, 2H, $H_{o\text{-Ph}}$), 8.16−8.21 (m, 6H, $H_{o\text{-Ph}}$), 8.664 and 8.721 (ABq, 2H, ^3J = 4.7, 4.7 Hz, $H_{\beta\text{-pyrrolic}}$), 8.73−8.77 (m, 4H, $H_{\beta\text{-pyrrolic}}$), 8.939 (d, 1H, ^4J = 0.7 Hz, $H_{3'(\beta\text{-pyrrolic})}$), 12.0 (br s, 1H, CO_2H). Assignments aided by COSY spectra. UV−vis (THF) λ_{max} (nm) (ϵ (10^3 M^{-1} cm^{-1})): 436 (279), 565 (16.8), 605 (6.73). FAB-LRMS *m*/*z* (%, assignment): cluster at 746−752, 746 (100, M^+). HRMS for M^+ ($C_{47}H_{30}N_4O_2Zn$): calcd, 746.1660; found, 746.1648.

*7. 3-(5′,10′,15′,20′-Tetraphenylporphyrin-2′-yl)allyl Hydroxide (**6**).* DIBAL−H (2.10 mL, 1.5 M in toluene, 3.15 mmol, 3.0 equiv) was added to a solution of **4** (750 mg, 1.05 mmol) in dry toluene (30 mL) under an argon atmosphere at 0 °C. After 30 min, the reaction was allowed to warm to room temperature. After another 30 min, the reaction was cooled to 0 °C, and MeOH (4.5 mL) was added followed by aqueous potassium sodium L-tartrate tetrahydrate (5 g in 150 mL). EtOAc (150 mL) was added, and the organic layer was washed with saturated aqueous $NaHCO_3$ and dried ($MgSO_4$), and the solvent was removed in vacuo. The residue was purified by column chromatography (silica, 45 mm_{dia} × 160 mm, CH_2Cl_2/Et_2O (99:1)), collecting the major red fraction. The product was precipitated with hexane to give **6** (618 mg, 88%) as a purple solid. ^{1}H NMR (400 MHz, $CDCl_3$, TMS, δ): −2.712 (s, 2H, NH), 4.118 (app t, 2H, ^3J = 5.2 Hz, CH_2OH), 6.292 (dd, 1H, ^3J = 15.6 Hz, ^4J = 0.8 Hz, $H_{3(ethenyl)}$), 7.478 (dt, 1H, ^3J = 15.6 Hz, ^3J = 5.5 Hz, $H_{2(ethenyl)}$), 7.70−7.83 (m, 12H, $H_{m,p\text{-Ph}}$), 8.06−8.10 (m, 2H, $H_{o\text{-Ph}}$), 8.18−8.21 (m, 6H, $H_{o\text{-Ph}}$), 8.736 (d, 1H, ^3J = 4.8 Hz, $H_{\beta\text{-pyrrolic}}$), 8.783 (d, 2H, ^3J = 4.8 Hz, $H_{\beta\text{-pyrrolic}}$), 8.80−8.85 (m, 4H, $H_{\beta\text{-pyrrolic}}$). UV−vis ($CH_2Cl_2$) λ_{max} (nm) (ϵ (10^3 M^{-1} cm^{-1})): 423 (240), 519 (17.1), 556 (6.25), 595 (5.27), 650 (2.71). FAB-LRMS *m*/*z* (%, assignment): cluster at 670−673, 671 (100, MH^+). HRMS for MH^+ ($C_{47}H_{35}N_4O_1$): calcd, 671.2811; found, 671.2775.

*8. 3-(5′,10′,15′,20′-Tetraphenylporphyrin-2′-yl)allyl Aldehyde (**7**).* Activated MnO_2 (367 mg, 4.22 mmol) was added to a solution of **6** (200 mg, 0.298 mmol) in dry CH_2Cl_2 (4.0 mL) and stirred at room temperature. After 19 h, TLC analysis (silica, CH_2Cl_2, R_f = 0.5) indicated all starting material had been consumed with the appearance of a new less polar band. The solution was filtered through Celite, and the solvent was removed in vacuo. The residue was purified by column chromatography (silica, 37 mm_{dia} × 140 mm, CH_2Cl_2/hexane (4:1)) to give **7** (183 mg, 89%) as a purple solid. ^{1}H NMR (400 MHz, $CDCl_3$, TMS, δ): −2.590 (br s, 2H, NH), 6.859 (dd, 1H, ^3J = 15.5 Hz, ^3J = 7.9 Hz, $H_{2(ethenyl)}$), 7.007 (d, 1H, ^3J = 15.5 Hz, $H_{3(ethenyl)}$), 7.72−7.85 (m, 12H, $H_{m,p\text{-Ph}}$), 8.11−8.13 (m, 2H, $H_{o\text{-Ph}}$), 8.18−8.21 (m, 6H, $H_{o\text{-Ph}}$), 8.784 and 8.794 (ABq, 2H, ^3J = 4.8, 4.8 Hz, $H_{\beta\text{-pyrrolic}}$), 8.842 (s, 2H, $H_{\beta\text{-pyrrolic}}$), 8.860 (s, 2H, $H_{\beta\text{-pyrrolic}}$), 8.996 (s, 1H, $H_{3'(\beta\text{-pyrrolic})}$), 9.209 (d, 1H, ^3J = 7.9 Hz, CHO). UV−vis (CH_2Cl_2) λ_{max} (nm) (ϵ (10^3 M^{-1} cm^{-1})): 434 (213), 525 (21.4), 567 (8.82), 604 (7.14), 661 (5.19). FAB-LRMS *m*/*z* (%, assignment): cluster centered at 669 (100, MH^+). HRMS for MH^+ ($C_{47}H_{33}N_4O_1$): calcd, 669.2654; found, 669.2625.

*9. 3-(2′-(5′,10′,15′,20′-Tetraphenylporphyrinato Zinc(II))yl)-allyl Aldehyde (**Zn-7**).* A solution of $Zn(OAc)_2{\cdot}2H_2O$ (79 mg, 359 μmol, 1.2 equiv) in MeOH (1.5 mL) was added to a solution of **7** (200 mg, 299 μmol) in $CHCl_3$ (20 mL) with stirring at room temperature. After 10 min, TLC analysis indicated that the reaction was complete with the appearance of a new more polar green band (R_f = 0.38, silica, CH_2Cl_2). Precipitation from methanol gave **Zn-7** (219 mg, 100%) as a purple microcrystalline powder. ^{1}H NMR (400 MHz, $CDCl_3$, TMS, δ): 6.632 (dd, 1H, ^3J = 15.4 Hz, ^3J = 8.0 Hz, $H_{2(ethenyl)}$), 6.963 (dd, 1H, ^3J = 15.6 Hz, ^4J = 0.7 Hz, $H_{3(ethenyl)}$), 7.67−7.82 (m, 12H, $H_{m,p\text{-Ph}}$), 8.11−8.13 (m, 2H, $H_{o\text{-Ph}}$), 8.07−8.09 (m, 6H, $H_{o\text{-Ph}}$), 8.85−8.92 (m, 7H, $6H_{\beta\text{-pyrrolic}}$ + $1H_{CHO}$), 9.208 (d, 1H, ^4J = 0.7 Hz, $H_{3'(\beta\text{-pyrrolic})}$). Assignments aided by COSY spectra. UV−vis (CH_2Cl_2) λ_{max} (nm) (ϵ (10^3 M^{-1} cm^{-1})) 437 (255), sh 522 (4.53), 560 (18.3), 601 (10.9). FAB-LRMS *m*/*z* (%, assignment): cluster at 730−737, 730 (95, M^+). HRMS for M^+ ($C_{47}H_{30}N_4OZn$): calcd, 730.1711; found, 730.1707.

*10. 2-Cyano-5-(2′-(5′,10′,15′,20′-tetraphenylporphyrinato Zinc-(II))yl)penta-2,4-dienoic Acid (**Zn-8**).* A solution of **Zn-7** (150 mg, 205 μmol), cyanoacetic acid (87 mg, 1.02 mmol, 5.0 equiv), and piperidine (490 μL, 5.0 mmol, 24 equiv) in methanol (15 mL) was heated at reflux temperature for 50 min under N_2. While the solution was cooled to room temperature, CH_2Cl_2 (50 mL) and H_2O (100 mL) were added, and the solution was shaken vigorously, adjusting the pH of the aqueous layer to pH = 2 with 2 M H_3PO_4 (3.0 mL). The organic layer was then carefully separated, and the CH_2Cl_2 was removed by azeotrope distillation using acetonitrile in vacuo. The crude product was precipitated from the resulting acetonitrile solution using H_2O and collected by filtration (#4 glass sinter). The solid was dissolved in $CHCl_3$ (aided by a little THF) and filtered (#4 glass sinter), and the product was precipitated with hexane to give **Zn-8** (137 mg, 84%) as a dark green solid. ^{1}H NMR (400 MHz,

DMSO-d_6, TMS, δ): 6.743 (d, 1H, $^3J = 14.7$ Hz, $H_{5(pentadienyl)}$), 7.203 (dd, 1H, $^3J = 14.7$, 11.7 Hz, $H_{4(pentadienyl)}$), 7.388 (d, 1H, $^3J = 11.7$ Hz, $H_{3(pentadienyl)}$), 7.76−7.91 (m, 12H, $H_{m,p\text{-Ph}}$), 8.07−8.23 (m, 8H, $H_{o\text{-Ph}}$), 8.72−8.75 (m, 6H, $H_{\beta\text{-pyrrolic}}$), 9.060 (s, 1H, $H_{3'(\beta\text{-pyrrolic})}$). Assignments aided by COSY spectra. UV−vis (THF) λ_{max} (nm) (ϵ (10^3 M^{-1} cm^{-1})) 334 (28.4), 414 (73.8), sh 444 (109), 466 (121), 572 (16.5), 622 (18.5). FAB-LRMS *m*/*z* (%, assignment): cluster at 797−803, 797 (100, M^+). HRMS for M^+ ($C_{50}H_{31}N_5O_2Zn$): calcd, 797.1769; found, 797.1767.

*11. Methyl 4-(trans-2′-(5″,10″,15″,20″-tetraphenyl porphyrin-2″-yl)ethen-1′-yl)-1,2-benzenedioate (**10**).* a. Wittig Reaction. A solution of TPPps **9** (400 mg, 432 μmol) and dimethyl 4-formylphthalate (288 mg, 1.30 mmol, 3.0 equiv) in $CHCl_3$ (50 mL) was heated to reflux under N_2. DBU (193 μL, 3.0 equiv) was added. After 15 min, TLC analysis indicated that all of the starting material had been consumed ($R_f = 0.28$, silica, CH_2Cl_2). The crude isomeric mixture was precipitated with methanol to give a cis/trans isomeric mixture of **10** as a purple powder (17% cis by ^{1}H NMR). ^{1}H NMR (400 MHz, $CDCl_3$, TMS, selected data only, δ): −2.718(s, NH_{cis}), −2.605 (s, NH_{trans}), 6.306 (d, $^3J = 11.6$ Hz, $H_{cis\text{-ethenyl}}$), 6.560 (dd, $^3J = 11.9$ Hz, $^4J = 1.1$ Hz, $H_{cis\text{-ethenyl}}$).

b. Isomerization. The isomeric mixture was dissolved in CH_2Cl_2 (30 mL), and I_2 (267 mg, 1.05 mmol, 2.4 equiv) was added. After the solution was stirred at room temperature for 3 h in darkness, excess saturated $Na_2S_2O_3$ (∼30 mL) was added, and stirring continued for 15 min. The organic layer was separated and dried ($MgSO_4$). The solvent was removed in vacuo to give *trans*-**10** (330 mg, 92%) as a purple solid. ^{1}H NMR (400 MHz, $CDCl_3$, TMS, δ): −2.602 (s, 2H, NH), 3.946 (s, 3H, CO_2CH_3), 4.047 (s, 3H, CO_2CH_3), 7.067 and 7.262 (ABq, 2H, $^3J = 16.2$, 15.9 Hz, $H_{2',1'}$), 7.361 (dd, 1H, $^3J = 8.2$ Hz, $^4J = 2.0$ Hz, ArH_5), 7.492 (d, 1H, $^4J = 1.6$ Hz, ArH_3), 7.72−7.84 (m, 13H, $12H_{m,p\text{-Ph}} + 1ArH_6$), 8.17−8.25 (m, 8H, $H_{o\text{-Ph}}$), 8.743 (d, 1H, $^3J = 4.8$ Hz, $H_{\beta\text{-pyrrolic}}$), 8.78−8.84 (m, 5H, $H_{\beta\text{-pyrrolic}}$), 8.985 (s, 1H, $H_{3''(\beta\text{-pyrrolic})}$). Assignments aided by COSY spectra. UV−vis (CH_2Cl_2) λ_{max} (nm) (ϵ (10^3 M^{-1} cm^{-1})) 292 (21.3), 428 (187), 524 (18.1), 564 (9.87), 600 (6.76), 663 (4.69). FAB-LRMS *m*/*z* (%, assignment): cluster at 832−836, 832 (75, M^+). HRMS for M^+ ($C_{56}H_{40}N_4O_4$): calcd, 832.3050; found, 832.3039.

*12. Methyl 4-(trans-2′-(2″-(5″,10″,15″,20″-tetraphenylporphyrinato Zinc(II))yl)ethen-1′-yl))-1,2-benzenedioate (**Zn-10**).* A solution of $Zn(OAc)_2 \cdot 2H_2O$ (47.0 mg, 216 μmol, 1.2 equiv) in MeOH (2.0 mL) was added to a solution of ester **10** (150 mg, 180 μmol) in $CHCl_3$ (10 mL) with stirring at room temperature. After 15 min, TLC analysis indicated that the reaction was complete with the appearance of a new more polar green band ($R_f = 0.23$, silica, CH_2Cl_2). Precipitation using MeOH gave **Zn-10** (134.7 mg, 84%) as a purple microcrystalline solid. ^{1}H NMR (400 MHz, $CDCl_3$, TMS, δ): 3.925 (s, 3H, CO_2CH_3), 4.036 (s, 3H, CO_2CH_3), 7.114 and 7.234 (ABq, 2H, $^3J = 15.8$, 14.4 Hz, $H_{2',1'}$), 7.366 (d, 1H, $^3J = 7.8$ Hz, ArH_5), 7.494 (s, 1H, ArH_3), 7.71−7.84 (m, 13H, $12H_{m,p\text{-Ph}} + 1ArH_6$), 8.15−8.27 (m, 8H, $H_{o\text{-Ph}}$), 8.833 (d, 1H, $^3J = 4.5$ Hz, $H_{\beta\text{-pyrrolic}}$), 8.88−8.95 (m, 5H, $H_{\beta\text{-pyrrolic}}$), 9.112 (s, 1H, $H_{3''(\beta\text{-pyrrolic})}$). Assignments aided by COSY spectra. UV−vis (CH_2Cl_2) λ_{max} (nm) (ϵ (10^3 M^{-1} cm^{-1})): 312 (23.9), 432 (228), 557 (22.0), 594 (10.0). FAB-LRMS *m*/*z* (%, assignment): cluster at 894−900, 894 (100, M^+). HRMS for M^+ ($C_{56}H_{38}N_4O_4Zn$): calcd, 894.2185; found, 894.2200.

*13. 4-(trans-2′-(2″-(5″,10″,15″,20″-Tetraphenylporphyrinato Zinc(II))yl)ethen-1′-yl))-1,2-benzenedicarboxylic Acid (**Zn-11**).* A solution of NaOH (179 mg, 20 equiv per CO_2Me, 4.48 mmol) in H_2O (1.2 mL) and MeOH (3.0 mL) was added to a refluxing solution of porphyrin **Zn-10** (100 mg, 112 μmol) in THF (6.0 mL) and MeOH (3.0 mL) under N_2. After 2 h, TLC analysis indicated that all of **Zn-10** had been consumed. After the solution was cooled to room temperature, CH_2Cl_2 (50 mL), H_2O (100 mL), and aqueous 2 M H_3PO_4 (3.5 mL) were added, and the solution was shaken vigorously in a separating funnel (pH ≈ 2.0), observing the porphyrin transferring from the aqueous layer to the organic layer. The organic layer was washed with H_2O (100 mL, containing 4 drops of aqueous 2 M H_3PO_4) and separated carefully. Acetone (50 mL) was added, and the CH_2Cl_2 was removed in vacuo. More acetone (50 mL) was added, and the volume was reduced to 20 mL. The product was precipitated from solution with H_2O (Milli-Q) and collected on a glass sinter (#4 glass sinter), washing with acetone/H_2O (1:1) to give **Zn-11** (94.5 mg, 98%) as a purple powder. ^{1}H NMR (400 MHz, DMSO-d_6, TMS, δ): 7.005 and 7.391 (ABq, 2H, $^3J = 16.0$, 15.9 Hz, $H_{2',1'}$), 7.446 (dd, 1H, $^3J = 7.8$ Hz, $^4J = 1.2$ Hz, ArH_5), 7.507 (br s, 1H, ArH_3), 7.725 (d, 1H, $^3J = 8.0$ Hz, ArH_6), 7.77−7.89 (m, 12H, $H_{m,p\text{-Ph}}$), 8.15−8.24 (m, 8H, $H_{o\text{-Ph}}$), 8.672 and 8.727 (ABq, 2H, $^3J = 4.7$, 4.6 Hz, $H_{\beta\text{-pyrrolic}}$), 8.727 and 8.763 (ABq, 2H, $^3J = 4.6$, 4.7 Hz, $H_{\beta\text{-pyrrolic}}$), 8.7403 (s, 2H, $H_{\beta\text{-pyrrolic}}$), 9.044 (s, 1H, $H_{3''(\beta\text{-pyrrolic})}$). 13.15 (br s, 2H, CO_2H). Assignments aided by COSY spectra. UV−vis (THF) λ_{max} (nm) (ϵ (10^3 M^{-1} cm^{-1})): 314(22.5), 437 (191), 565 (18.4), 602 (7.89). FAB-LRMS *m*/*z* (%, assignment): cluster at 866−873, 866 (100, M^+). HRMS for M^+ ($C_{54}H_{34}N_4O_4Zn$): calcd, 866.1875; found, 866.1872.

*14. 4-(trans-2′-(2″-(5″,10″,15″,20″-Tetraphenylporphyrinato Zinc(II))yl)ethen-1′-yl)-1-benzaldehyde (**Zn-12**).* A solution of $Zn(OAc)_2 \cdot 2H_2O$ (71 mg, 322 μmol, 1.2 equiv) in MeOH (2.0 mL) was added to a solution of **12** (200 mg, 269 μmol) in $CHCl_3$ (10 mL) with stirring at room temperature. After 20 min, TLC analysis indicated that the reaction was complete. Precipitation with methanol gave **Zn-12** (218 mg, 100%) as a purple powder. ^{1}H NMR (400 MHz, $CDCl_3$, TMS, δ): 7.177 and 7.256 (ABq, 2H, $^3J = 16.0$, 16.0 Hz, $H_{1',2'}$), 7.336 (d, 2H, $^3J = 8.0$ Hz, $H_{3,5}$), 7.771 (m, 14H, $12H_{m,p\text{-Ph}} + 2H_{2,6}$), 8.217 (m, 8H, $H_{o\text{-Ph}}$), 8.815 and 8.894 (ABq, 2H, $^3J = 4.8$, 4.8 Hz, $H_{\beta\text{-pyrrolic}}$), 8.903 and 8.935 (ABq, 2H, $^3J = 4.8$, 4.8 Hz, $H_{\beta\text{-pyrrolic}}$), 8.913 (s, 2H, $H_{\beta\text{-pyrrolic}}$), 9.134 (d, 1H, $^4J = 0.8$ Hz, $H_{3''}$), 9.918 (s, 1H, CHO). UV−vis (CH_2Cl_2) λ_{max} (nm) (ϵ (10^3 M^{-1} cm^{-1})): 321 (28.1), 364 (24.3), 433 (231), 525 (5.54), 558 (24.8), 595 (12.7). FAB-LRMS *m*/*z* (%, assignment): cluster at 806−813, 806 (100, M^+). HRMS for M^+ ($C_{53}H_{34}N_4OZn$): calcd, 806.2024; found, 806.2002.

*15. 2-Cyano-3-[4′-(trans−2″-(2‴-(5‴,10‴,15‴,20‴-tetraphenylporphyrinato Zinc(II))yl) ethen-1″-yl)-phenyl]-acrylic Acid (**Zn-13**).* A solution of **Zn-12** (150 mg, 186 μmol), cyanoacetic acid (313 mg, 3.68 mmol, 20 equiv), and piperidine (1.02 mL, 10.3 mmol, 55 equiv) in methanol (15 mL) was heated at reflux temperature for 15 h under argon. After the solution was cooled to room temperature, CH_2Cl_2 (∼100 mL) and H_2O (200 mL) were added, and the solution was shaken vigorously, adjusting the pH of the aqueous layer to pH = 2 with 2 M H_3PO_4 (7.0 mL). The organic layer was then washed a second time with H_2O (200 mL) containing of 2 M H_3PO_4 (1.0 mL, pH = 2). The organic layer was then carefully separated, and the product was precipitated with acetonitrile, removing the CH_2Cl_2 by azeotrope distillation in vacuo to give **Zn-13** (133.3 mg, 82%) as a dark purple powder. ^{1}H NMR (400 MHz, DMSO-d_6, TMS, δ): 7.143 and 7.354 (ABq, 2H, $^3J = 15.9$, 15.9 Hz, $H_{1'',2''}$), 7.415 (d, 2H, $^3J = 8.5$ Hz, $H_{3',5'}$), 7.75−7.89 (m, 12H, $H_{m,p\text{-Ph}}$), 8.012 (d, 2H, $^3J = 8.5$ Hz, $H_{2',6'}$), 8.15−8.23 (m, 8H,

$H_{o\text{-}Ph}$), 8.285 (s, 1H, $H_{3,acrylic}$), 8.656 and 8.723 (ABq, 2H, ^3J = 4.7, 4.6 Hz, $H_{\beta\text{-}pyrrolic}$), 8.722 and 8.760 (ABq, 2H, ^3J = 4.7, 4.7 Hz, $H_{\beta\text{-}pyrrolic}$), 8.738 (s, 2H, $H_{\beta\text{-}pyrrolic}$), 9.036 (s, 1H, $H_{3'''}$). Assignments aided by COSY and LR-COSY spectra. UV−vis (THF) λ_{max} (nm) (ϵ (10^3 M^{-1} cm^{-1})): 362 (27.4), 437 (136), 568 (21.9), 608 (14.8). FAB-LRMS *m*/*z* (%, assignment): cluster at 871−881, 873 (100, M^+). HRMS for M^+ ($C_{56}H_{35}N_5O_2Zn$): calcd, 873.2082; found, 873.2063.

Results and Discussion

A. Synthetic Studies. The synthesis of these β-substituted porphyrin carboxylic acids was readily achieved from the free-base (FB) β-formylporphyrin TPP−CHO **1** using established procedures.[43] The α-cyanoacetic acid derivative **Zn-3** was obtained in three steps by metalation of **1** using the acetate method [46] to give the metallo derivative **Zn-1** (Scheme 1), followed by Knoevenagel condensation with cyanoacetic acid, affording the piperidine salt **Zn-2** in good yield. Subsequent treatment of **Zn-2** with phosphoric acid (pH ≈ 2) gave the desired carboxylic acid **Zn-3** without demetalation. Both the piperidine salt proton resonances/integrals of **Zn-2** and the acid proton of **Zn-3** were observable in the ^{1}H NMR spectra. In the piperidine salt **Zn-2**, a broadened baseline was observed under the β-pyrrolic resonances; this was presumed to be due to the NH^+ resonance.

The synthesis of the acrylic acid derivative **Zn-5** has previously been reported to proceed via the Wittig reaction of nickel β-formylporphyrin[47] with ethyl (triphenylphosphoranylidene)acetate to give **Ni-4**,[48] and subsequent demetalation of this with sulfuric acid yielded **4**.[49] Metalation using zinc acetate, followed by hydrolysis with potassium hydroxide, gave **Zn-5** (no characterization of **Zn-5** was reported).[50] A more direct approach to **Zn-5** has been achieved here with the conversion of the FB β-formylporphyrin **1** directly to the FB porphyrin ethyl acrylate **4**. FB **4** has also been previously synthesized by Effenberger and Strobel using a phosphonium salt but not fully characterized.[51] The Wittig reaction of aldehyde **1** with the ylide ethyl (triphenylphosphoranylidene)acetate in refluxing toluene gave a cis/trans mixture (2:3) of **4** in excellent yield. Isomerization of this mixture with I_2 then gave **4** in 90% overall yield. The metalation of **4** to give **Zn-4**, followed by ester hydrolysis, quantitatively gave **Zn-5**. The ^{1}H NMR spectra of **4** and **Zn-4** are consistent with those reported,[49−51] and the resulting acid **Zn-5** has now been fully characterized by ^{1}H NMR, FAB HRMS, and UV−vis spectroscopy.

Synthesis of the α-cyanopentadienoic acid **Zn-8** was achieved via the DIBAL−H reduction of ester **4** to alcohol **6** using a similar procedure to that of Effenberger and Strobel.[51] MnO_2 oxidation of **6** to aldehyde **7**, followed by metalation, gave **Zn-7**. An alternative synthesis of aldehyde **7** has also been previously reported by Ishkov et al. via the Wittig reaction of β-formylporphyrin TPP−CHO **1** with the protected ylide of 2-bromoethanal, followed by hydrolysis to an inseparable cis/trans mixture of aldehyde **7**.[52] The ^{1}H NMR data of **6** and **7** is consistent with those published.[51,52] The Knoevenagel condensation of **Zn-7** with cyanoacetic acid then gave the pentadienoic acid **Zn-8** in good yield (84%).

The conversion of β-formyl porphyrin TPP−CHO **1** into the phosphonium salt **9**[43] allowed the synthesis of **Zn-11** and **Zn-13** (Scheme 2). Using the Wittig chemistry of phosphonium salt **9** with an excess of dimethyl 4-formylphthalate[53,54] allowed the efficient synthesis of **10**, after I_2 isomerization. Metalation then hydrolysis gave **Zn-11** in excellent yield. In an analogous fashion, the Wittig reaction of **9** with terephthaldialdehyde afforded the building block **12**.[44] Quantitative metalation of **12** to give **Zn-12** and the subsequent condensation with cyanoacetic acid gave the desired α-cyanoacetic acid product **Zn-13**. Generally all the final acid products were purified via precipitation from appropriate solvents. Chromatography of the acids was avoided since this generally resulted in irretrievable loss of the compounds. All compounds were characterized by ^{1}H NMR spectroscopy, UV−vis spectroscopy, and FAB HRMS and afforded ^{1}H NMR spectra typical of substituted tetraphenylporphyrins with no unusual features. Where necessary, ^{1}H NMR assignments were aided by two-dimensional NMR spectra. Often a small long-range ^4J coupling (∼0.8 Hz) was observed between the closest vinylic proton at the nearest β-pyrrolic proton on the porphyrin ring. Also, in the majority of cases, the broadened acid proton resonance was readily visible (and integrateable) in DMSO-d_6. The HRMS data was as expected for the desired compounds.

B. Electronic Spectroscopy. The UV−vis spectra of the metalloporphyrins ZnTTP, **Zn-3**, **Zn-5**, **Zn-8**, **Zn-11**, and **Zn-13** in THF solvent are shown in Figure 2, and the absorption maxima and extinction coefficients for the Soret- and Q-bands of the derivatized porphyrins are listed in Table 1. The metalloporphyrins show a series of bands between 400 and 650 nm due to $\pi-\pi^*$ absorptions of the conjugated macrocycle [55] that are red-shifted with respect to the Soret- and Q-bands of ZnTPP, and the α-cyanoacetic acids, **Zn-3**, **Zn-8**, and **Zn-13**, are red-shifted with respect to those of **Zn-5** and **Zn-11**. The Q-bands of **Zn-3** and **Zn-13** also show a significant red shift, and the cyanoporphyrins generally have higher molar extinction coefficients in this region. The absorption spectra of the porphyrins adsorbed onto 9-μm-thick TiO_2 electrodes are similar to those of the corresponding solution spectra but exhibit a small red shift due to the interaction of the anchoring groups with the surface.

The emission spectra of metalloporphyrins **Zn-3**, **Zn-5**, **Zn-8**, **Zn-11**, and **Zn-13**, shown in Figure 3, were obtained at room temperature in THF solution. The emission maxima (Table 1) are independent of the excitation wavelength between 400 and 600 nm, and the spectra show characteristic vibronic bands for **Zn-5**, **Zn-11**, and **Zn-13** at around 630 and 675 nm similar to those reported in other Zn porphyrins.[56] Porphyrins **Zn-3** and **Zn-8** display only a broad single band at 670 and 688 nm, respectively. The excitation spectra, monitored at 675 nm, exhibit intense Soret and Q-bands that correspond with the ground-state absorption spectra, indicating the presence of a single emitting species in each case. No emission spectra are observed for the porphyrins adsorbed onto 9-μm-thick TiO_2 layers as a consequence of electron injection from the excited singlet state of the porphyrin into the conduction band of the TiO_2.[57] The emission from the argon-degassed solution of **Zn-3**, **Zn-5**, **Zn-8**, **Zn-11**, and **Zn-13** at 298 K excited at 532 nm in the $\pi-\pi^*$ absorption band decays as a single exponential with a time constants τ given in Table 1. The emission time constants are several orders of magnitude greater than the electron injection rate into the conduction band of the TiO_2.[24]

The changes in the electronic absorption spectra with the nature of the linker can be understood by examining the calculated orbital energies for ZnTPP, **Zn-3**, and **Zn-5**. DFT calculations (B3LYP) using the basis set 3-21G* show that for ZnTPP the highest occupied molecular orbital (HOMO) and the HOMO − 1 are split by 0.14 eV, and the unoccupied MOs are doubly degenerate. The HOMO−LUMO gap is calculated at 2.97 eV. When porphyrin ring substituents increase the splitting between the key filled orbitals or lift the degeneracy present in

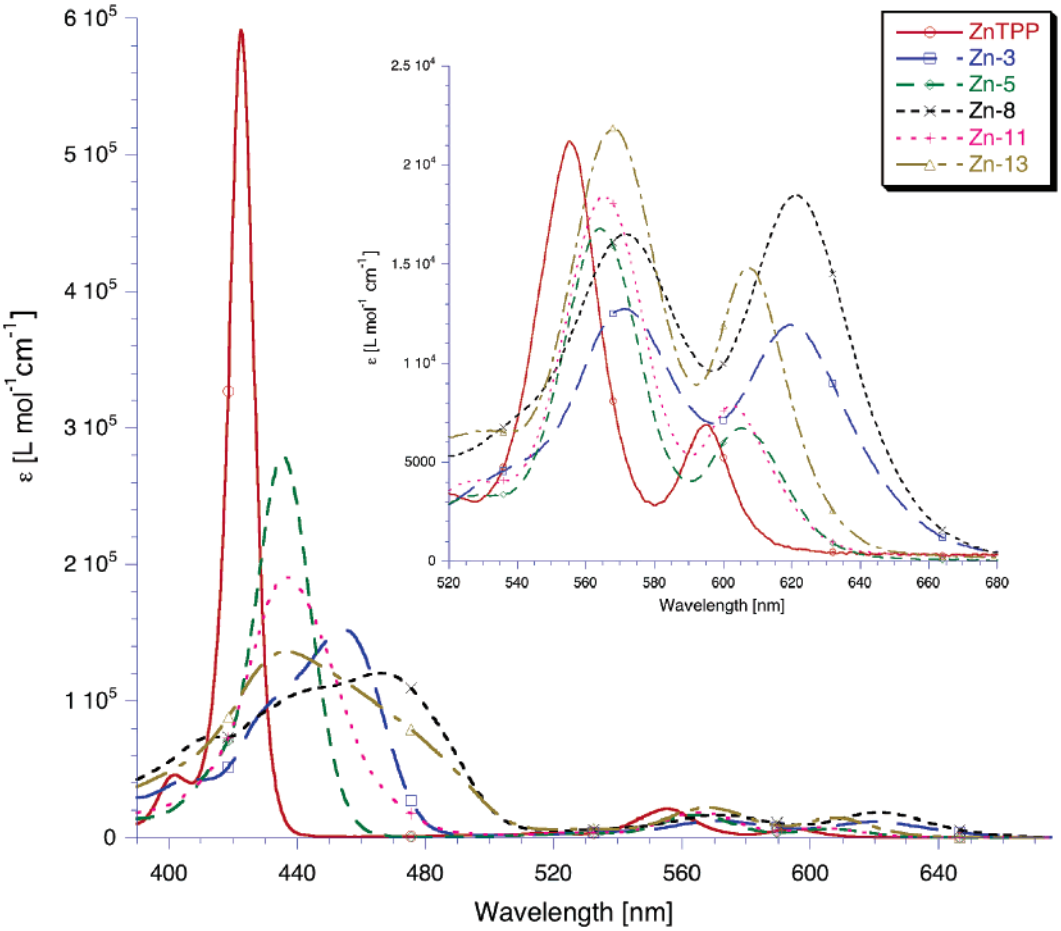

Figure 2. UV−vis absorption spectra of zinc tetraphenylporphyrin (ZnTPP), **Zn-3**, **Zn-5**, **Zn-8**, **Zn-11**, and **Zn-13** in THF.

TABLE 1: Electronic Absorption/Emission and Electrochemical Data for Zinc Porphyrins

	absorption[a] λ_{max}, nm (ϵ, 10^3 M^{-1} cm^{-1})	emission[b] λ_{max}, nm	τ, ns	E_{ox},[c] V	E_{ox}*,[d] V
Zn-3	sh 429 (92.4), 455 (153), 571 (12.7) 620 (11.9)	670	4	0.45	−1.40
Zn-5	436 (279), 565 (16.8), 605 (6.73)	628, 671	3	0.39	−1.46
Zn-8	414 (73.8), sh 444 (109), 466 (121), 572 (16.5), 622 (18.5)	688	4	0.43	−1.43
Zn-11	437 (191), 656 (18.4), 602 (7.89)	625, 674	3	0.38	−1.48
Zn-13	437 (136), 568 (21.9), 608 (14.8)	629, 678	4	0.39	−1.46

[a] Absorption data were obtained in THF solution at 298 K. [b] Emission spectra were obtained at 298 K in THF by exciting at 570 nm. [c] Electrochemical measurements were performed at 298 K using square wave voltammetry on solutions in DMF containing 0.1 M $TBAPF_6$ as the supporting electrolyte. Potentials are quoted with respect to ferrocene (Fc^+/Fc). [d] Approximate values for the excited-state redox potentials extracted from the potentials of the ground-state couples and the zero excitation energy (E_{0-0}).

the unoccupied orbitals, the Q-transition gains in intensity.[34,58−60] The electron-withdrawing substituent has a stabilizing effect on the energies of all of the frontier molecular orbitals (FMOs), relative to their energies in ZnTPP (Table 2). The degeneracy of the LUMO and LUMO + 1 is broken, with the LUMO extending out onto the substituent (Figure 4) and being further stabilized by the stronger electron-withdrawing cyanocarboxylate group in **Zn-3** than in **Zn-5**; the LUMO + 2 is also stabilized in this manner.

DFT and TDDFT studies on the optical absorptions of meso-substituted porphyrins have shown that the Soret- and Q-absorptions of these porphyrins each correspond to two overlapping one-electron transitions involving the four FMOs.[61] TDDFT singlet calculations have been performed on ZnTPP, **Zn-3**, and **Zn-5** at the 3-21G* level. The ZnTPP calculation shows two pairs of transitions in the visible region. The two at 2.18 eV (569 nm) are comprised of the four FMOs, and the two at 2.45 eV (506 nm) are comprised of the four FMOs and the HOMO − 2. They all have oscillator strengths of below 0.05. Two strong transitions are predicted at 3.44 eV (360 nm); these correspond to the Soret band. The largest coefficient of these bands belongs to the HOMO − 2 → LUMO (40%) and HOMO − 2 → LUMO + 1 (41%) transitions, respectively. Transitions in the near-UV are largely limited to oscillator strengths of below 0.05. At energies of less than 4 eV (310 nm), these transitions comprise lower orbitals up to the HOMO − 5; at energies above 4 eV, orbitals to HOMO − 10 and the LUMO + 2 are involved.

In general, upon substitution there is a red shift and an increase in the calculated oscillator strengths of the visible transitions. This reflects the higher absorptions in this region, in the experimental UV−vis spectra of the substituted porphyrins. The sum of the oscillator strengths for these four transitions increases from 0.014 in ZnTPP, to 0.040 for **Zn-5**, and to 0.108 for **Zn-3**.

The TDDFT calculation on **Zn-5** shows splitting of the two pairs of visible transitions. The lowest energy transition is slightly red-shifted (0.08 eV) from that of ZnTPP (Table 3).

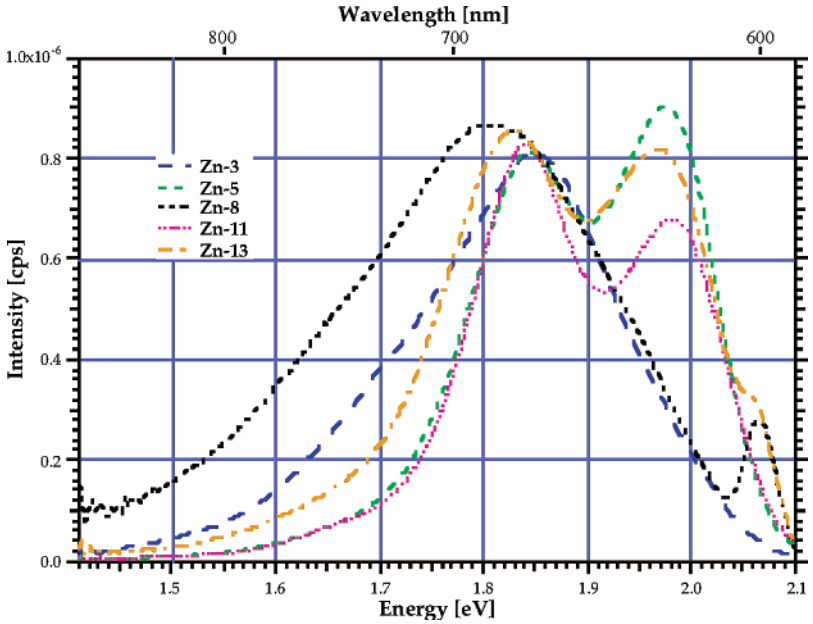

Figure 3. Emission spectra of porphyrins **Zn-3**, **Zn-5**, **Zn-8**, **Zn-11**, and **Zn-13** in THF solution. The excitation wavelength was 570 nm.

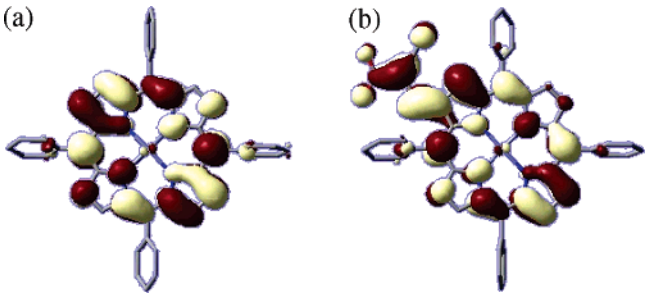

Figure 4. LUMOs of (a) ZnTPP (doubly degenerate) and (b) **Zn-3**.

TABLE 2: Calculated Energies of Frontier Molecular Orbitals for ZnTPP, Zn-5, and Zn-3

	ZnTPP	**Zn-5**	**Zn-3**
E(LUMO + 2)/eV	−0.52	−1.17	−1.61
E(LUMO + 1)/eV	−2.10	−2.20	−2.29
E(LUMO)/eV	−2.10	−2.37	−2.67
E(HOMO)/eV	−5.06	−5.20	−5.28
E(HOMO − 1)/eV	−5.20	−5.31	−5.47

TABLE 3: Experimental and Calculated Red Shifts for Zn-5 and Zn-3 Relative to ZnTPP

	Zn-5 red shifts, eV		**Zn-3** red shifts, eV	
	experimental	calculated	experimental	calculated
Q(0,0)	−0.05	−0.08	−0.10	−0.20
B(0,0)	−0.12	−0.28	−0.24	−0.48
		−0.21		−0.40

All four of the visible transitions now involve the HOMO − 2. The calculated Soret transitions are also split and red-shifted; these transitions now involve MOs from the HOMO − 3 to the LUMO + 2. A third strong calculated transition ($f = 0.49$) appears to the blue of the two Soret transitions at 3.31 eV (375 nm). In the near-UV region, other calculated transitions are red-shifted and enhanced in intensity (Supporting information).

The TDDFT calculation on **Zn-3** shows that the increase in the oscillator strengths of the visible transitions is more pronounced, and the lowest calculated transition has a larger red shift relative to ZnTPP of 0.20 eV. The splitting of the calculated visible transitions is larger for **Zn-3** than that for **Zn-5**. The calculated Soret transitions are red-shifted by 0.48 and 0.40 eV. This compares with an experimental red shift of 0.24 eV (Table 3). The HOMO − 2 and LUMO + 2 are involved in both transitions, and the lower-energy transition involves the HOMO − 3. The largest coefficient of the more intense, higher-energy transition involves the stabilized LUMO + 2. Calculated transitions in the near-UV are also red-shifted and enhanced in intensity.

C. ATR-FTIR Spectroscopy. ATR-FTIR spectroscopy has been shown to be a powerful tool to extract structural information for the metal complexes adsorbed onto the TiO_2 surface.[62,63] In particular, by comparison of the characteristic stretching modes of the −COOH and −CN groups of a solid-state spectrum with those for molecules adsorbed on a surface, the mode of attachment of porphyrins to the surface can be determined. ATR-FTIR spectra of metalloporphyrins **Zn-3**, **Zn-5**, **Zn-8**, **Zn-11**, and **Zn-13** were measured both as a solid and when adsorbed on TiO_2 films, and the spectra for **Zn-3** are shown in Figure 5. The spectra of the solid samples all show a strong and intense absorption at around 1700 cm^{-1} due to the υ(C═O) of the carboxylic acid group.[64] The strong bands at 1520, 1490, 1484, 1439, 1334, and 997 cm^{-1} are due to the ring stretching modes of the porphyrin. The IR band at around 1595 cm^{-1} is due to characteristic υ(C═C) stretching frequency. The α-cyanoacetic acids porphyrins **Zn-3**, **Zn-8**, and **Zn-13** display a medium intensity band at 2223 cm^{-1} due to the υ(CN) group stretching frequency.

ATR-FTIR spectra of the adsorbed complex on TiO_2 film show the presence of strong carboxylate asymmetric 1597 cm^{-1} $\upsilon(-COO^-_{as})$ and symmetric 1383 cm^{-1} $\upsilon(-COO^-_{s})$ bands. Porphyrins, **Zn-3**, **Zn-8**, and **Zn-13**, i.e., those that contain an α-cyano group, also display a very weak υ(NC) band at 2214 cm^{-1}. The presence of carboxylate bands in the IR spectra of adsorbed complexes on TiO_2 show that the carboxylic acid groups are adsorbed on the TiO_2 surface in a dissociated form. Indeed, on the basis of this IR data and the recent theoretical studies on the interaction of formic acid and sodium formate on the anatase (101) surface,[65] it is likely that the binding occurs through a bidentate bridging mode to the TiO_2 surface.[12]

D. Electrochemical Properties. Cyclic voltammetry was used to determine the redox potentials of the porphyrins. All porphyrins show chemically reversible waves for a one-electron

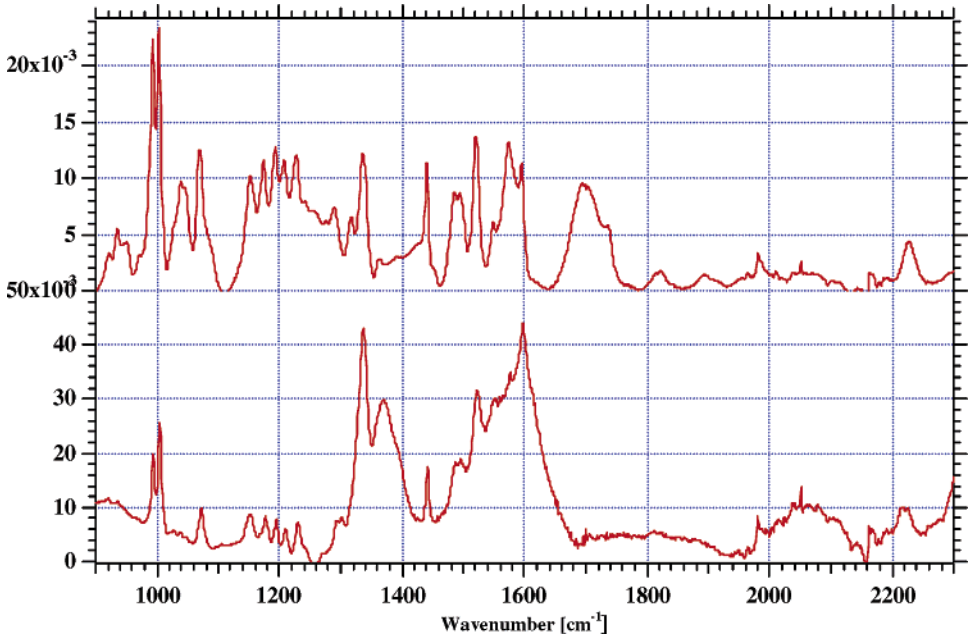

Figure 5. ATR-FTIR spectra of **Zn-3** measured as a pure solid (top trace) and that of the dye adsorbed onto a 3-μm-thick TiO_2 film (bottom trace). The latter spectrum was obtained by subtracting the IR spectrum of the untreated film from that of the dye-coated film.

oxidation and reduction, and the measured redox potentials are listed in Table 1. The oxidation potentials of **Zn-3** and **Zn-8** are positively shifted by about 60 mV compared with the other porphyrins as a result of the strong electron-withdrawing nature of the CN group. **Zn-13**, the other cyano porphyrin, does not show this shift, probably as a result of the phenyl vinylene spacer substituent, which attenuates the effect. Additional one-electron oxidations are present at a potential of about 0.8 V (not included in Table 1), corresponding to the formation of the dication from the radical cation.[66] There are also reversible one-electron reductions at around −1.7 V due to the reduction of the porphyrin ring and a second one-electron reduction at about −2.0 V as a result of the reduction of the porphyrin anion. The CVs obtained for the dyes adsorbed onto TiO_2 film show little change from those observed in THF solution despite the fact that nanocrystalline TiO_2 films are conductive only in the accumulation regime and are electronically blocking under reverse bias due to the electronic band gap. The phenomenon has been observed previously for fullerene and triphenylamine on nanocrystalline oxides [67,68] and is attributed to lateral charge hopping between neighboring adsorbed molecules, in this case between the adsorbed porphyrin molecules. This is not surprising in view of the highly delocalized porphyrin structures and the fact that electronic communication between porphyrin molecules in self-assembled multilayers has been previously observed.[69]

E. Light-Induced Charge Separation at the Porphyrin/TiO_2 Interface. Excitation of the porphyrin molecules with visible light leads to an electronically excited state that undergoes electron-transfer quenching as a consequence of electrons being injected into the conduction band of the semiconductor. The oxidized porphyrin is subsequently reduced back to the ground state (S) by the electron donor (I^-) present in the electrolyte. The electrons in the conduction band collect at the back-current collector and subsequently pass through the external circuit to arrive at the counter electrode. The photocurrents generated as a result of this charge separation were measured as a function of wavelength in the 400−800 nm region, and the resulting photocurrent action spectra are shown in Figure 6. The shapes of these spectra are slightly broader but clearly follow the shape of the corresponding absorption

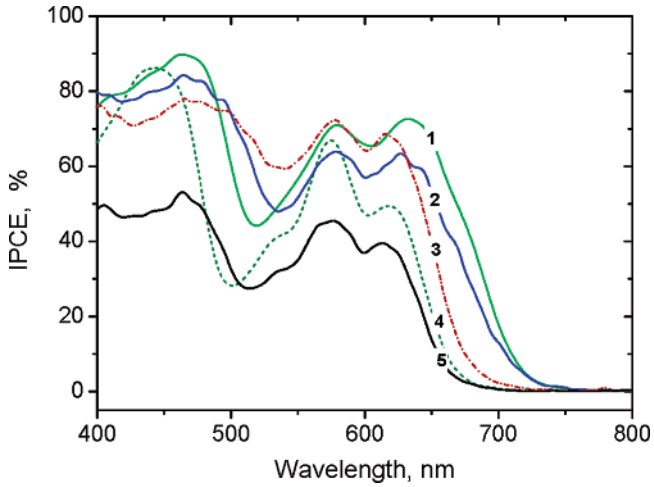

Figure 6. Photocurrent action spectra obtained with **Zn-3** (1), **Zn-8** (2), **Zn-13** (3), **Zn-5** (4), and **Zn-11** (5) anchored on nanocrystalline TiO_2 films.

spectra shown in Figure 2. In particular, the red shifts seen in the Q-band absorptions of **Zn-3** and **Zn-8** are also seen in the photoaction spectra of these molecules. In addition, the cyanoporphyrins exhibit enhanced IPCE values over most of the spectral range. For example, the maximum IPCE value achieved at around 463 nm (Soret band) for **Zn-3** of 89% corresponds to almost unity quantum yield (electrons per absorbed photon) when light losses are taken into account. An IPCE value of more than 70% is also obtained for the Q-band for this compound. The photovoltaic data for the porphyrin-sensitized cells are given in Table 4, where it is seen that the better IPCE values associated with the cyanoporphyrins are reflected in the higher short circuit currents of these cells.

The most efficient sensitizer, **Zn-3**, yields an overall efficiency of 5.2%, a value that is the best thus far obtained for porphyrin-sensitized cells. For macrocyclic organic dyes such as phthalocyanines or porphyrins, solution aggregation as a result of π-stacking might lead to an adsorption of aggregates onto the TiO_2. One way to prevent this is to add a bulky molecule such as chenodeoxycholic acid to the **Zn-3** solution during the

TABLE 4: Photovoltaic Performance of Dye-Sensitized Cells Using Different Zn Porphyrins as Sensitizers[a]

metalloporphyrin	V_{oc}, mV	J_{sc}, mA/cm^2	η, %
Zn-3	566	13.5	5.2
Zn-5	555	10.9	4.0
Zn-8	535	11.4	4.0
Zn-11	509	7.2	2.4
Zn-13	530	11.0	3.7

[a] The illumination is 100 mW/cm^2. The electrolyte is 0.6 M BMII, 0.1 M LiI, 0.5 M *t*BuPy, and 0.05 M I_2 in a mixture of acetonitrile and valeronitrile (1:1 in volume ratio).

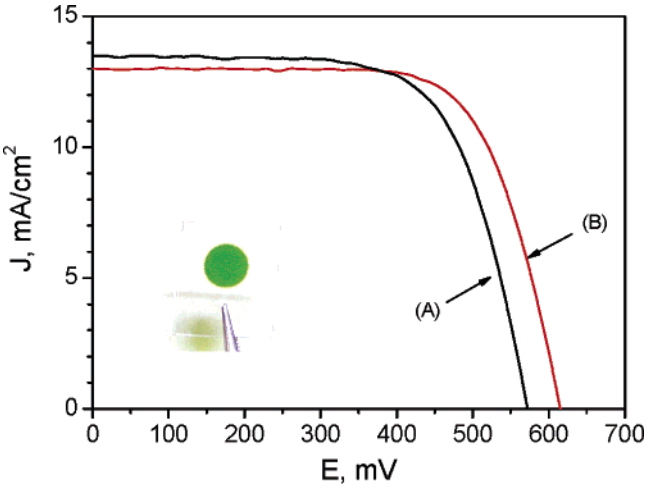

Figure 7. Photocurrent−voltage characteristics of the nanocrystalline photoelectrochemical cell sensitized with **Zn-3** (A) with an overall efficiency of 5.2%. The response shown in curve B was achieved from a cell in which the dye sensitization of the TiO_2 was carried out in the presence of 2 mM chenodeoxycholic acid in THF solvent. The overall cell efficiency for this cell is 5.6% (V_{oc} = 610 mV, J_{sc} = 13 mA/cm^2, ff = 0.70). A light source simulating global AM 1.5 solar radiation was employed, the incident intensity being 100 mW/cm^2. The insert shows a **Zn-3**-coated TiO_2 film.

sensitization process.[32] Indeed, a chenodeoxycholic acid concentration of 0.2 mM in the dye solution does result in an increase in cell performance (η = 5.6%), as shown in Figure 7, but only by a small amount, suggesting that aggregation is not a significant factor in influencing the efficiency of the cell. Nevertheless, to the best of our knowledge, this is the highest value reported until now for a porphyrin/TiO_2 light-harvesting system. Attempts to further improve the overall efficiency of these functionalized porphyrin-sensitized cells will concentrate on tuning the dye deposition methods and the composition of the electrolytes.

Conclusions

A series of novel intense green porphyrins containing carboxylate anchoring groups have been shown to have potential as light sensitizers in TiO_2 solar cells. DFT and TDDFT calculations have shown that the presence of electron-withdrawing moieties on the substituent modulates the electronic absorption spectrum through stabilization of the energies of the LUMO and LUMO + 2. The extension of the LUMO and LUMO + 2 onto the substituent implies that occupation of these MOs offers the possibility of electron transfer from the substituent to the TiO_2 surface. The ground- and excited-state redox potentials show that the porphyrins possess suitable potentials to inject electrons into the TiO_2 substrate, yielding 85% IPCE. Among the reported porphyrins, the green **Zn-3** shows the highest power conversion efficiency obtained so far in nanocrystalline films. These findings open up new avenues for further improving the efficiency of nanocrystalline solar cells for practical utility, by engineering porphyrins with a slightly decreased gap between the HOMO and the LUMO that absorb in the visible and the near-IR regions of the solar spectrum.

Acknowledgment. We acknowledge financial support of this work by the Swiss Federal Office for Energy (OFEN), the U. S. Air Force Research Office under contract number F61775-00-C0003, and the New Zealand Foundation for Research, Science and Technology New Economy Research Fund contracts MAUX0014 and MAUX0202. We thank Dr. Marie Jirousek and P. Comte for their kind assistance in obtaining photovoltaic data and TiO_2 electrodes.

Supporting Information Available: Electrochemical data and the DFT calculation showing calculated transitions and intensities of these sensitizers. This material is available free of charge via the Internet at http://pubs.acs.org.

References and Notes

(1) Kavarnos, G. J. *Fundamentals of Photoinduced Electron Transfer*; VCH: Weinheim, New York, 1993.
(2) O'Regan, B.; Grätzel, M. *Nature* **1991**, *353*, 737.
(3) Grätzel, M. *Nature* **2001**, *414*, 338.
(4) Grätzel, M. *J. Photochem. Photobiol., A* **2004**, *164*, 3.
(5) Grätzel, M. *J. Sol−Gel Sci. Technol.* **2001**, *22*, 7.
(6) Nazeeruddin, M. K.; Kay, A.; Rodicio, I.; Humphry-Baker, R.; Muller, E.; Liska, P.; Vlachopoulos, N.; Grätzel, M. *J. Am. Chem. Soc.* **1993**, *115*, 6382.
(7) Bach, U.; Lupo, D.; Comte, P.; Moser, J. E.; Weissortel, F.; Salbeck, J.; Spreitzer, H.; Grätzel, M. *Nature* **1998**, *395*, 583.
(8) Nazeeruddin, M. K.; Pechy, P.; Renouard, T.; Zakeeruddin, S. M.; Humphry-Baker, R.; Comte, P.; Liska, P.; Cevey, L.; Costa, E.; Shklover, V.; Spiccia, L.; Deacon, G. B.; Bignozzi, C. A.; Grätzel, M. *J. Am. Chem. Soc.* **2001**, *123*, 1613.
(9) Kruger, J.; Plass, R.; Grätzel, M.; Matthieu, H. J. *Appl. Phys. Lett.* **2002**, *81*, 367.
(10) Wang, P.; Zakeeruddin, S. M.; Moser, J. E.; Nazeeruddin, M. K.; Sekiguchi, T.; Grätzel, M. *Nat. Mater.* **2003**, *2*, 402.
(11) Grätzel, M.; Moser, J.-E. In *Electron Transfer in Chemistry*; Balzani, V., Gould, I., Eds.; Wiley-VCH: Weinheim, 2001; Vol. V, pp 589−644.
(12) Nazeeruddin, M. K.; Humphry-Baker, R.; Officer, D. L.; Campbell, W. M.; Burrell, A. K.; Grätzel, M. *Langmuir* **2004**, *20*, 6514.
(13) Vittadini, A.; Selloni, A.; Rotzinger, F. P.; Grätzel, M. *J. Phys. Chem. B* **2000**, *104*, 1300.
(14) Anderson, J. M. *Aust. J. Plant Physiol.* **1999**, *26*, 625.
(15) Ben Shem, A.; Frolow, F.; Nelson, N. *Photosynth. Res.* **2004**, *81*, 239.
(16) Lammi, R. K.; Wagner, R. W.; Ambroise, A.; Diers, J. R.; Bocian, D. F.; Holten, D.; Lindsey, J. S. *J. Phys. Chem. B* **2001**, *105*, 5341.
(17) Liu, Z. M.; Yasseri, A. A.; Lindsey, J. S.; Bocian, D. F. *Science* **2003**, *302*, 1543.
(18) Imahori, H.; Mori, Y.; Matano, Y. *J. Photochem. Photobiol., C* **2003**, *4*, 51.
(19) Choi, M. S.; Yamazaki, T.; Yamazaki, I.; Aida, T. *Angew. Chem., Int. Ed.* **2004**, *43*, 150.
(20) Gust, D.; Moore, T. A.; Moore, A. L. *Acc. Chem. Res.* **2001**, *34*, 40.
(21) Dabestani, R.; Bard, A. J.; Campion, A.; Fox, M. A.; Mallouk, T. E.; Webber, S. E.; White, J. M. *J. Phys. Chem.* **1988**, *92*, 1872.
(22) Vlachopoulos, N.; Liska, P.; Mcevoy, A. J.; Grätzel, M. *Surf. Sci.* **1987**, *189*, 823.
(23) Kalyanasundaram, K.; Vlachopoulos, N.; Krishnan, V.; Monnier, A.; Grätzel, M. *J. Phys. Chem.* **1987**, *91*, 2342.
(24) Tachibana, Y.; Haque, S. A.; Mercer, I. P.; Durrant, J. R.; Klug, D. R. *J. Phys. Chem. B* **2000**, *104*, 1198.
(25) Odobel, F.; Blart, E.; Lagree, M.; Villieras, M.; Boujtita, H.; El Murr, N.; Caramori, S.; Bignozzi, C. A. *J. Mater. Chem.* **2003**, *13*, 502.
(26) Cherian, S.; Wamser, C. C. *J. Phys. Chem. B* **2000**, *104*, 3624.
(27) Jasieniak, J.; Johnston, M.; Waclawik, E. R. *J. Phys. Chem. B* **2004**, *108*, 12962.
(28) Ma, T. L.; Inoue, K.; Yao, K.; Noma, H.; Shuji, T.; Abe, E.; Yu, J. H.; Wang, X. S.; Zhang, B. W. *J. Electroanal. Chem.* **2002**, *537*, 31.
(29) Ma, T. L.; Inoue, K.; Noma, H.; Yao, K.; Abe, E. *J. Photochem. Photobiol., A* **2002**, *152*, 207.

(30) Campbell, W. M.; Burrell, A. K.; Officer, D. L.; Jolley, K. W. *Coord. Chem. Rev.* **2004**, *248*, 1363.
(31) Fungo, F.; Otero, L. A.; Sereno, L.; Silber, J. J.; Durantini, E. N. *J. Mater. Chem.* **2000**, *10*, 645.
(32) Kay, A.; Grätzel, M. *J. Phys. Chem.* **1993**, *97*, 6272.
(33) Chen, C. T.; Yeh, H. C.; Zhang, X. Q.; Yu, J. W. *Org. Lett.* **1999**, *1*, 1767.
(34) Gouterman, M. *J. Chem. Phys.* **1959**, *30*, 1139.
(35) Vosko, S. H.; Wilk, L.; Nusair, M. *Can. J. Phys.* **1980**, *58*, 1200.
(36) Becke, A. D. *Phys. Rev. A* **1988**, *38*, 3098.
(37) Burke, K.; Perdew, J. P.; Wang, Y. In *Electronic Density Functional Theory: Recent Progress and New Directions*, Proceedings of the International Workshop on Electronic Density Functional Theory: Recent Progress and New Directions, Nathan, Australia, July 14−19, 1996; Dobson, J. F., Vignale, G., Das, M. P., Eds.; Plenum Press: New York, 1998, pp 81−111
(38) Becke, A. D. *J. Chem. Phys.* **1993**, *98*, 5648.
(39) Nguyen, K. A.; Day, P. N.; Pachter, R. *J. Phys. Chem. A* **2000**, *104*, 4748.
(40) Nguyen, K. A.; Day, P. N.; Pachter, R. *J. Chem. Phys.* **1999**, *110*, 9135.
(41) van Gisbergen, S. J. A.; Rosa, A.; Ricciardi, G.; Baerends, E. J. *J. Chem. Phys.* **1999**, *111*, 2499.
(42) Stratmann, R. E.; Scuseria, G. E.; Frisch, M. J. *J. Chem. Phys.* **1998**, *109*, 8218.
(43) Bonfantini, E. E.; Burrell, A. K.; Campbell, W. M.; Crossley, M. J.; Gosper, J. J.; Harding, M. M.; Officer, D. L.; Reid, D. C. W. *J. Porphyrins Phthalocyanines* **2002**, *6*, 708.
(44) Belcher, W. J.; Burrell, A. K.; Officer, D. L.; Reid, D. C. W.; Scott, S. M. *Journal of Porphyrins and Phthalocyanines* **2002**, *6*, 720.
(45) Frisch, M. J.; Trucks, G. W.; Schlegel, H. B.; Scuseria, G. E.; Robb, M. A.; Cheeseman, J. R.; Montgomery, Jr., J. A.; Vreven, T.; Kudin, K. N.; Burant, J. C.; Millam, J. M.; Iyengar, S. S.; Tomasi, J.; Barone, V.; Mennucci, B.; Cossi, M.; Scalmani, G.; Rega, N.; Petersson, G. A.; Nakatsuji, H.; Hada, M.; Ehara, M.; Toyota, K.; Fukuda, R.; Hasegawa, J.; Ishida, M.; Nakajima, T.; Honda, Y.; Kitao, O.; Nakai, H.; Klene, M.; Li, X.; Knox, J. E.; Hratchian, H. P.; Cross, J. B.; Bakken, V.; Adamo, C.; Jaramillo, J.; Gomperts, R.; Stratmann, R. E.; Yazyev, O.; Austin, A. J.; Cammi, R.; Pomelli, C.; Ochterski, J. W.; Ayala, P. Y.; Morokuma, K.; Voth, G. A.; Salvador, P.; Dannenberg, J. J.; Zakrzewski, V. G.; Dapprich, S.; Daniels, A. D.; Strain, M. C.; Farkas, O.; Malick, D. K.; Rabuck, A. D.; Raghavachari, K.; Foresman, J. B.; Ortiz, J. V.; Cui, Q.; Baboul, A. G.; Clifford, S.; Cioslowski, J.; Stefanov, B. B.; Liu, G.; Liashenko, A.; Piskorz, P.; Komaromi, I.; Martin, R. L.; Fox, D. J.; Keith, T.; Al-Laham, M. A.; Peng, C. Y.; Nanayakkara, A.; Challacombe, M.; Gill, P. M. W.; Johnson, B.; Chen, W.; Wong, M. W.; Gonzalez, C.; Pople, J. A. *Gaussian 03*; Gaussian, Inc.: Wallingford, CT, 2004.
(46) Smith, K. M. *Porphyrins and Metalloporphyrins*; Elsevier: Amsterdam: 1975.
(47) Callot, H. J. *Tetrahedron* **1973**, *29*, 899.
(48) Callot, H. J.; Castro, B.; Selve, C. *Tetrahedron Lett.* **1978**, *19*, 2877.
(49) Selve, C.; Niedercorn, F.; Nacro, M.; Castro, B.; Gabriel, M. *Tetrahedron* **1981**, *37*, 1893.
(50) Selve, C.; Niedercorn, F.; Nacro, M.; Castro, B.; Gabriel, M. *Tetrahedron* **1981**, *37*, 1903.
(51) Effenberger, F.; Stobel, H. *Chem. Ber.* **1993**, *126*, 1683.
(52) Ishkov, Y. V.; Zhilina, Z. I.; Grushevaya, Z. V. *Zh. Org.Khim.* **1993**, *29*, 2270.
(53) Baker, W. R.; Rosenberg, S. H.; Fung, K. L. A.; Rockway, T. W.; Fakhoury, S. A.; Garvey, D. S.; Donner, B. G.; O'Connor, S. J.; Prasad, R. N.; Shen, W.; Stout, D. M.; Sullivan, G. M.; Abbott Laboratories. International Patent Application 241, 1996.
(54) Ainsworth, A. T.; Smith, D. G.; Beecham Group, Ltd., U. K. European Patent Application 89, 1980.
(55) Kalyanasundaram, K. *Photochemistry of Polypyridine and Porphyrin Complexes*; Academic Press: London: 1992.
(56) Tait, C. D.; Holten, D.; Barley, M. H.; Dolphin, D.; James, B. R. *J. Am. Chem. Soc.* **1985**, *107*, 1930.
(57) Nazeeruddin, M. K.; Humphry-Baker, R.; Grätzel, M.; Murrer, B. A. *Chem. Commun.* **1998**, 719.
(58) LeCours, S. M.; DiMagno, S. G.; Therien, M. J. *J. Am. Chem. Soc.* **1996**, *118*, 11854.
(59) Spellane, P. J.; Gouterman, M.; Antipas, A.; Kim, S.; Liu, Y. C. *Inorg. Chem.* **1980**, *19*, 386.
(60) Gouterman, M. *Porphyrins* **1978**, *3*, 1.
(61) Cramariuc, O.; Hukka, T. I.; Rantala, T. T. *Chem. Phys.* **2004**, *305*, 13.
(62) Duffy, N. W.; Dobson, K. D.; Gordon, K. C.; Robinson, B. H.; McQuillan, A. J. *Chem. Phys. Lett.* **1997**, *266*, 451.
(63) Finnie, K. S.; Bartlett, J. R.; Woolfrey, J. L. *Langmuir* **1998**, *14*, 2744.
(64) Nazeeruddin, M. K.; Humphry-Baker, R.; Liska, P.; Grätzel, M. *J. Phys. Chem. B* **2003**, *107*, 8981.
(65) Persson, P.; Lunell, S.; Ojamae, L. *Int. J. Quantum Chem.* **2002**, *89*, 172.
(66) Burrell, A. K.; Officer, D. L.; Reid, D. C. W.; Scott, S. M.; Gordon, K. C. *J. Porphyrins Phthalocyanines* **2000**, *4*, 626.
(67) Bonhóte, P.; Gogniat, E.; Tingry, S.; Barbe, C.; Vlachopoulos, N.; Lenzmann, F.; Comte, P.; Grätzel, M. *J. Phys. Chem. B* **1998**, *102*, 1498.
(68) Papageorgiou, N.; Grätzel, M.; Enger, O.; Bonifazi, D.; Diederich, F. *J. Phys. Chem. B* **2002**, *106*, 3813.
(69) Savenije, T. J.; Goossens, A. *Phys. Rev. B* **2001**, *64*, 115323.